Check for updates

Building the Himalaya from tectonic to earthquake scales

Luca Dal Zilio [ID] [1 ✉], *György Hetényi* [ID] [2], *Judith Hubbard[3] and Laurent Bollinger[4]*

Abstract | Convergence of the Indian Plate towards Eurasia has led to the building of the Himalaya, the highest mountain range on Earth. Active mountain building involves a complex interplay between permanent tectonic processes and transient seismic events, which remain poorly understood. In this Review, we examine the feedbacks between long-term tectonic deformation (over millions of years) and the seismic cycle (years to centuries) in the Himalaya. We discuss how surface morphology of the Himalaya indicates that the convergence is largely accommodated by slip on the Main Himalayan Thrust plate boundary fault, which developed in the roots of the mountain range over millions of years. At shorter (decadal) timescales, tectonic geodesy reveals that elastic strain is periodically released via earthquakes. We use examples from earthquake cycle models to suggest that partial ruptures could primarily occur in the downdip region of the Main Himalayan Thrust. Great (Mw 8+) Himalayan earthquakes are more commonly associated with complete megathrust ruptures, which release accumulated residual strain. By synthesizing numerous observations that co-vary along strike, we highlight that tectonic structures that developed over millions of years can influence stress accumulation, structural segmentation, earthquake rupture extent and location, and, consequently, the growth of the mountain range.

Orogen
A belt of the Earth's crust involved in the formation of mountains, owing to tectonic plate convergence.

[1]Seismological Laboratory, California Institute of Technology, Pasadena, California, CA, USA.

[2]Institute of Earth Sciences, University of Lausanne, Lausanne, Switzerland.

[3]Earth Observatory of Singapore, Nanyang Technological University, Singapore, Singapore.

[4]Commissariat à l'Energie Atomique et aux Energies Alternatives (CEA), Arpajon, France.

✉e-mail: dalzilio@caltech.edu

The Himalayan orogen, standing at 7,000–8,000 m, represents a striking topographic boundary between the near-sea-level Ganges and Brahmaputra plains to the south and the 4,500–5,000-m-high Tibetan Plateau to the north. The Himalaya are underlain by one of the largest continental megathrusts on Earth, and, consequently, the region experiences large earthquakes[1] that cause extensive damage and death tolls in both the Himalaya and the densely populated foreland plains (for example, 2015 Mw 7.8 Gorkha, 2005 Mw 7.6 Kashmir, 1950 Mw 8.5–8.7 Assam, 1934 Mw 8.4 Bihar–Nepal, 1905 Mw 7.8 Kangra, 1897 Mw 8.2–8.3 Assam–Shillong Plateau). However, large Himalayan earthquakes have long recurrence intervals[2] (hundreds of years), and the limited instrumental record leaves large gaps in our scientific understanding of how the long-term deformation links to and informs earthquake hazard.

Over geological timescales (10^4–10^7 years), crustal deformation is usually described as a continuous, quasi-steady process accommodated by a combination of viscous deformation at depth and brittle deformation in the upper crust[3]. However, the occurrence of strong ($6 < Mw < 7$), major ($7 < Mw < 8$) and great (Mw 8+) earthquakes attests to the episodic nature of upper crustal shortening and associated transient processes[4] (such as dynamic weakening, viscous flow, post-seismic creep,

landscape modification and fluid migration). These transient processes are impacted by structural geometries, lithologies, stress states and the presence of fluids, which often evolve over long timescales.

Long-term deformation processes, therefore, influence all parts of the seismic cycle, including interseismic stress-strain accumulation, seismic slip events (earthquakes), post-seismic deformation and non-linear viscous deformation at depth[5]. In turn, deformation across multiple earthquake cycles integrates to produce long-term deformation and shapes tectonic structures, from the topography to the roots of the orogen. Furthermore, crustal deformation and topography are influenced by climate and surface denudation[6–10], and, in turn, topography and weathering can alter monsoonal patterns and long-term climate[11,12]. These multiple feedback cycles result in a non-linear, dynamically evolving system that is coupled across a large number of spatial and temporal scales.

In this Review, we discuss the interplay between the long-term tectonics and short-term seismicity across the Himalayan range, and we describe how such interplay affects the seismic behaviour and topography. As they are subaerial, the Himalaya are one of the best places on Earth to observe and analyze the geologic evolution and natural hazards of a mountain belt. We discuss how large-scale

REVIEWS

Key points

- The Himalayan mountain belt is a unique subaerial orogenic wedge characterized by tectonically rapid, ongoing crustal shortening and thickening, intense surface denudation and recurrent great (Mw 8+) earthquakes.

- The history of the orogen has been investigated from long (million-year) to short (seconds to days) timescales using a variety of geological and geophysical techniques.

- The magnitude 7.8 Gorkha earthquake and aftershocks were monitored by extensive local geophysical networks, providing a unique set of observations of a major Himalayan earthquake and the Himalayan seismic cycle.

- Observations across the Himalaya reveal along-strike segmentation patterns at various temporal scales, controlled by inherited tectonic complexities developed over millions of years.

- Developing a complete understanding of deformation across timescales from seconds to millions of years requires an integrated, interdisciplinary effort.

and long-term tectonic deformations contribute to structural segmentation and earthquake generation, and how the Himalayan topography responds to stress perturbations across different stages of the seismic cycle. We identify current knowledge gaps and future opportunities towards better understanding how the Himalaya deform in space and time, which has implications for seismic hazard. Although the features described in this Review are based on observations from the Himalaya, the interaction of multiscale processes is applicable to that in other continent–continent collision zones.

Long-term tectonic deformation

The Himalaya are a natural laboratory that provide a unique opportunity for studying mountain-building processes, earthquakes and deep dynamics related to continent–continent collision. Understanding these processes requires reconstruction of both crustal shortening patterns (developed over millions of years) and present-day crustal structures. In this section, we discuss the geological architecture of the Himalayan range and review how geophysical explorations are used to investigate the structure and tectonic processes at work.

Geological background. Over the last 70 to 50 million years, northward drift of India and its collision with Eurasia has led to the construction of the Himalayan arc and Tibetan Plateau[13–18] (FIG. 1). The Tibetan Plateau, as a whole, has accommodated most of the north–south shortening (estimated at more than 1,400 km) since the onset of India–Eurasia collision, and the Himalayan arc represents the main collisional front of this orogen[16] (FIG. 1a). Before collision with Eurasia at ~50 million years ago (Ma)[19–22], the Indian Plate converged rapidly at rates of ≥14 cm per year for a period of 20 million years[20,23,24] (FIG. 1a). Shortly after collision, buoyancy of the Indian continental margin slowed convergence to ~4–5 cm per year, a rate that has persisted since that time[19,23–27] (FIG. 1b).

The India–Eurasia collision has resulted in a complex wedge, with the accretion from north to south of three tectonic domains defined by a combination of stratigraphy, faults and topography[16] — the High Himalaya, the Lesser Himalaya and the Sub-Himalaya (FIG. 2). The High Himalaya represents the high, rugged part of the range. Its northern boundary is roughly marked by the North Himalayan Normal Fault[28], also

called the South Tibetan Detachment[29]. Rocks north of the South Tibetan Detachment are known as the Tethyan Himalaya, and consist of late Precambrian to early Palaeozoic sedimentary and metasedimentary rocks[29,30] and thick Permian to Cretaceous continental margin sequences[16,31]. The southern boundary of the High Himalaya is defined as a transition from steeper, higher topography in the north to a lower topography in the Lesser Himalaya to the south. The High Himalaya exposes the Greater Himalayan crystalline sequence and, in some regions, parts of the largely Proterozoic metasedimentary Lesser Himalayan sequence, which crops out from the Main Boundary Thrust (MBT) in the south to the Main Central Thrust (MCT) in the north[16,32] (FIG. 2a).

Geographically, the Lesser Himalaya domain is bounded by the MBT in the south to the MCT in the north and exposes Lesser Himalayan sequence rocks[31]. We note that Lesser Himalayan sequence rocks can be found in both the Lesser and the High Himalaya, which are defined based on structure and topography, rather than lithology. To the south, the Sub-Himalaya is the youngest part of the system, spanning from the frontal fault (the Main Frontal Thrust, or MFT) to the MBT; in this case, the stratigraphic and geographic definitions coincide. The Sub-Himalaya is built out of Siwaliks sedimentary foreland basin sediments and records the last couple of million years of shortening history[33].

Himalayan shortening has been largely accommodated along three main fault systems: the MFT, the MBT and the MCT (FIG. 2b). The most recently active faults are those in the Sub-Himalaya, which contains between 1 and ~5 subparallel fault strands[34]. Together, these faults are sometimes called the MFT system, with the MFT being the southernmost and youngest fault in the set. The MFT is also the most active surface-breaching fault associated with the Himalaya[35]. The MBT is roughly parallel to the range front, began to slip at ~11 Ma and was active during the Pleistocene[36]. The MCT is older: it formed at ~22–18 Ma and might have remained episodically active[37] since. As the MCT is refolded, its primary trace lies within the High Himalaya, but it is also exposed around klippen within the Lesser Himalaya. The MCT records the bulk of geological shortening in the Himalaya, accommodating from 140 km to >500 km of displacement[38–40].

The MFT, the MBT and the primary exposure of the MCT are interpreted to merge at depth with the Main Himalayan Thrust (MHT), the north dipping basal décollement that separates the Indian and Eurasian plates and accommodates most of the plate convergence (FIG. 2b). The MHT is the largest (~2,400 km long) and one of the fastest slipping (~17–21 mm per year) continental megathrusts on Earth[41], and, thus, represents the primary seismic hazard in the Himalaya.

Deep geophysical signatures. Although much of the tectonic history in an orogen is either eroded or buried to substantial depth, subsurface tectonic information can be discovered through geophysical imaging techniques. Imaging the subsurface geometry of a fault is easier if there is either an extensive damage zone or a marked contrast in physical properties between the footwall and

---

Seismic cycle
Repeating process during which mechanical stress slowly builds up on a fault over a long period (interseismic period, years to centuries), is rapidly released in an earthquake (coseismic period, seconds to tens of seconds) and experiences a period of stress adjustment following coseismic slip (post-seismic relaxation, weeks to months).

Surface denudation
Loss of landscape mass leading to a reduction in elevation and relief of a landscape, driven by erosion and chemical weathering.

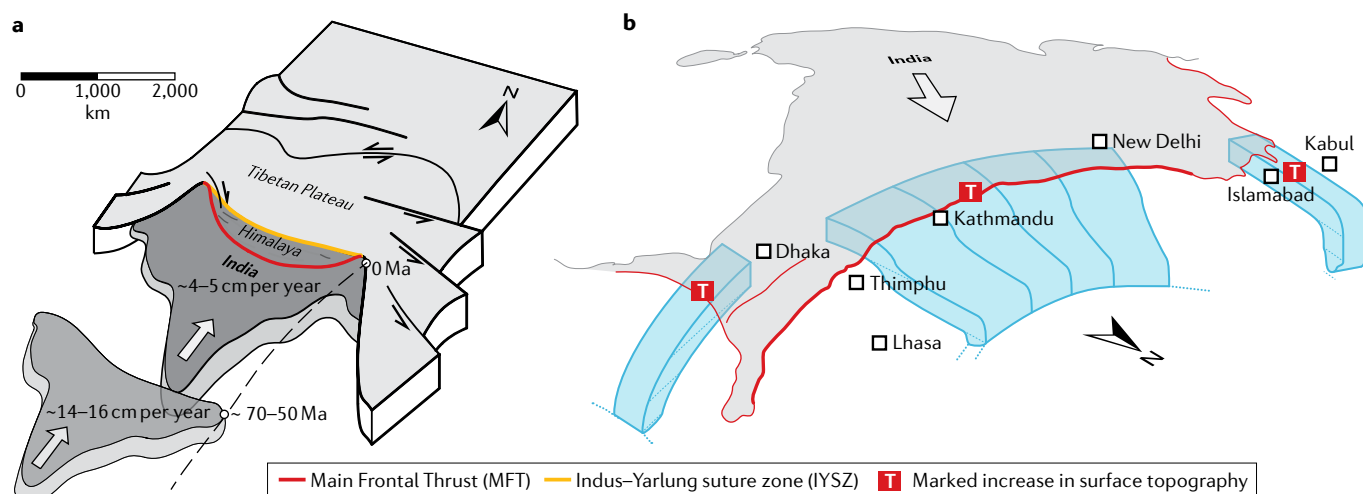**Footwall**
The body of rock below a non-vertical fault.

Main Frontal Thrust (MFT) — Indus–Yarlung suture zone (IYSZ) **T** Marked increase in surface topography

Fig. 1 | **Long-term convergence and collision of India with Eurasia and geometry of the subducting plate.**
a | The northward drift of India and its collision with Eurasia over the last ~70 million years. **b** | Present-day geometry of the subducting Indian Plate that differs beneath the Himalayan arc (underthrusting) and the surrounding orogens (subduction), as inferred from geophysical explorations. Red lines indicate the frontal thrust faults (the Main Frontal Thrust is shown by the thicker line) and 'T' symbols locate the marked increase in surface topography (>1 km). Panel **a** adapted with permission from REF.[17], Elsevier.

the hanging wall. In ocean–continent subduction zones, for example, the large contrasts between the wedge sediments, the downgoing oceanic crust and the forearc mantle facilitate geophysical imaging. This imaging is further aided by the heterogeneous effects of fluids[42]. However, in the Himalayan continent–continent setting, the megathrust (the MHT) is located within recently underthrust sediments, making imaging more difficult. Furthermore, the temporal and spatial migration of the MHT within this sedimentary stack has built a complex orogenic wedge through duplexing and material transfer across the fault zone[43,44]. Therefore, neither a primary nor an omnipresent contrast of physical properties is expected across the MHT, which can, thus, be imaged only indirectly or by high-resolution active seismic methods.

Multichannel seismic reflection acquired as part of the Sino-American INDEPTH survey in the Yadong-Gulu rift successfully imaged the MHT[45,46] (FIG. 2). The INDEPTH survey results showed a band of reflections, aligned linearly with a northward dip of ~12°, corresponding to the MHT mid-crustal ramp beneath and north of the High Himalaya[45,46]. Owing to difficulties in obtaining permits and access to carry out extensive surveys, this survey remains the best high-resolution, active-source geophysical data illuminating the deep crustal structure. Further mapping can be done by indirect geophysical methods, such as various seismological and electromagnetic experiments, which are feasible, as the MHT hosts microseismic activity and fluids that can be observed with passive geophysical surveys.

Fluids in particular provide a mechanism for observing and interpreting the structure and state of rocks at depth, and evidence for the presence of fluids in the Himalaya has been locally documented at the surface by fluid inclusions in minerals[47]. Magnetotelluric sounding in Nepal has revealed an electrically highly conductive zone south of the High Himalaya that can be explained by about 3% aqueous fluid porosity[48]. Fluids likely originate, in part, from metamorphic dehydration reactions of underthrust Indian sediments and basement, and then percolate upward through the deformed brittle media, accumulating within or below the possibly impermeable MHT shear zone at ~20 km depth, near the ramp–flat transition[48]. Notably, the presence of fluids at the MHT has been documented by broadband seismology exploiting converted waves, an approach sensitive to sharp velocity variations across sub-horizontal interfaces. Fluids at the MHT reduce shear-wave velocities, so that the megathrust appears as a low-velocity zone[49–55], with variable depth (ca. 10–18 km)[52]. Converted seismic waves also allow the interpretation of locally anisotropic rock structure, which is coherent with the top-to-the-south thrusting of the MHT[56].

The depth range of the MHT also hosts microseismic activity in both the interseismic and post-seismic periods, likely related to fluids and stress accumulation[57,58]. The interseismic period includes microseismic swarms[59]. These transient events can be observed to migrate at 35–50 m per day and could be related to either fluid migration or geodetically unresolved slow slip events[60]. Structurally, some active clusters in both the interseismic[60] and post-seismic[61–63] periods can be interpreted as individual splays or ramp faults at mid-crustal depths. Dense monitoring over large regions could help track and understand fluid migration patterns, with possible implications for how strain accumulates and is released through different parts of the seismic cycle.

Shallow morphotectonic signatures. The geomorphology and drainage patterns above active faults and related growing folds provide insight into the ongoing tectonics. River incision, waterfalls, flights of abandoned fluvial terraces, palaeo-lake formation and/or abandonment, and angular unconformities are all indicative of

---

Hanging wall
The body of rock above a non-vertical fault.

tectonic deformation[64–70]. These geomorphic markers can be used to determine tectonic uplift and shortening in the Sub-Himalaya and the evolution of the landscape over timescales of thousands of years[64,65,69].

Abandoned terraces that sit above the rivers draining the Sub-Himalaya record uplift along the MFT[64]. Although this fault is discontinuous along the length of the Himalaya, profiles typically reveal a frontal anticline that has risen steadily during the Holocene. For example, in central Nepal, the uplift rate has been measured at a maximum of ~11 mm per year[64]. By interpreting the geometry of the subsurface fault and basal décollement, terrace-based uplift profiles can be used to infer shortening rates. This approach yields a long-term slip rate on the MFT of ~21 ± 1.5 mm per year at the Bagmati River in central Nepal[64].

Short-term deformation
Over the past three decades, satellite geodesy has revolutionized our view of crustal deformation between, during and after earthquakes (interseismic, coseismic and post-seismic phases) (FIG. 3). Combining these techniques with seismological and geological methods can illuminate where faults accumulate elastic strain, and the partitioning between seismic and aseismic slip in time and space. In this section, we discuss how these tools have provided new insights into monitoring crustal deformation and earthquake-related processes in the Himalaya, including advantages and limitations. We then discuss historical major (Mw ~7–8) and great (Mw 8+) Himalayan earthquakes, with a special focus on the 2015 Mw 7.8 Gorkha earthquake, which is the most recent and best instrumented major seismic event in the region.

Interseismic shortening. Interseismic deformation across the Himalaya has been documented by the Global Navigation Satellite System (GNSS), enabling the community to assess surface motion and extrapolate secular velocities[71–75]. Early studies based on limited Global Positioning System (GPS) data defined a clockwise rotation of the Indian Plate relative to Asia, with ~44 mm
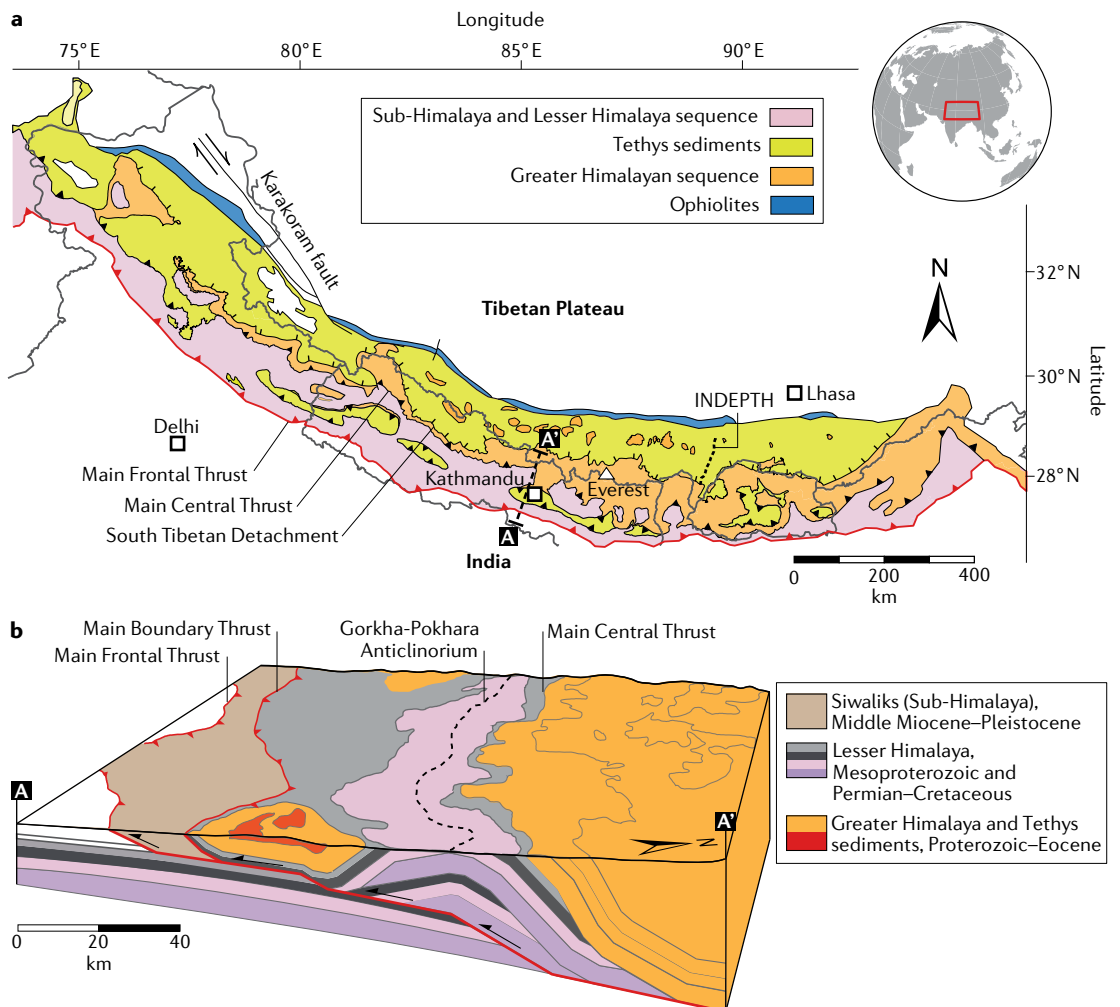

Fig. 2 | **Geological map and 3D cross section of the Himalaya. a** | Simplified geological map of the Himalayan arc showing the major structural units and major faults. Black dashed lines indicate the location of the cross section (panel **b**; labelled A–A') and the INDEPTH seismic reflection line. **b** | Simplified 3D cross section of the Himalaya showing the surface geology, the geometry of the Main Himalayan Thrust and the tectonic units at depth. Panel **a** adapted with permission from REF.[207], Geological Society of America. Panel **b** adapted from REF.[118], CC BY 4.0 (https://creativecommons.org/licenses/by/4.0/).
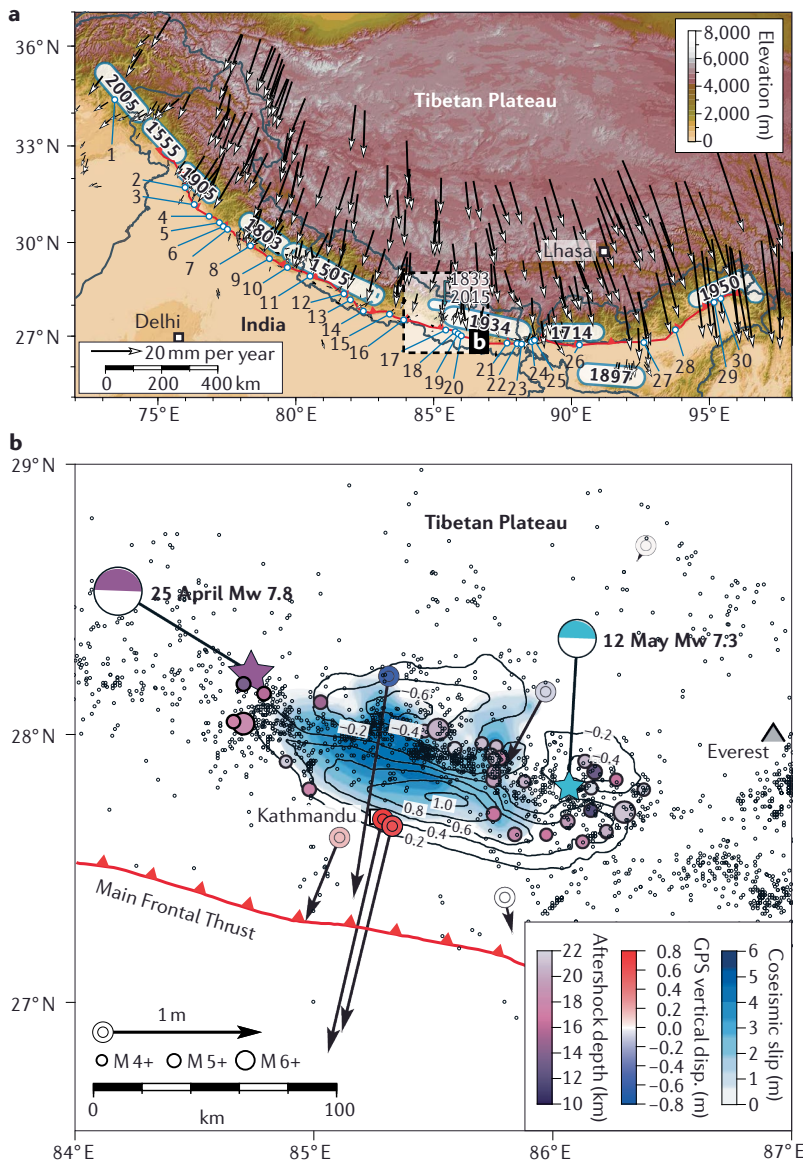
Fig. 3 | **Plate convergence velocity field and characteristics of the 2015 Mw 7.8 Gorkha earthquake.** **a** | Global Positioning System (GPS) velocities showing Himalayan convergence. Black vectors indicate GPS velocities spanning the 1990s to 2015 in an India-fixed reference frame[208,209]. White transparent patches show the approximate location and size of major and great historical earthquakes on the Main Himalayan Thrus[1,210]. White circles with light blue outline locate palaeoseismological sites along the Himalayan front[2,70] (1, Muzaffarabad; 2, Hajipur; 3, Bhatpur; 4, Chandigarh; 5, Kala Amb; 6, Rampur Ganda; 7, Dehra Dun; 8, Lal Dhang; 9, Ramnagar; 10, Chor Ghalia; 11, Mohan River; 12, Botechaur; 13, Suketal; 14, Koilabas; 15, Bandel Pokhari; 16, Tribeni; 17, Bagmati; 18, Mahra Khola; 19, Bardibas; 20, Charnath; 21, Damak; 22, Hokse; 23, Tokla; 24, Singimuni; 25, Chalsa; 26, Sarpang; 27, Nameri; 28, Harmutti; 29, Marang; 30, Pasighat). **b** | White-to-blue colour map indicates the coseismic slip distribution[188] on the Main Himalayan Thrust from the 2015 Mw 7.8 Gorkha earthquake. Stars denote epicentres of the main shock (Mw 7.8) and the largest (Mw 7.3) aftershock, and the corresponding purple and light blue focal mechanisms are the centroid moment tensor solutions, respectively[211]. Circles indicate aftershock locations, magnitude and depth[111]. Black contour lines indicate the coseismic displacement field ALOS-2 satellite (positive towards satellite)[113]. Blue-to-red coloured circles indicate measured vertical GPS coseismic displacements and black arrows indicate horizontal displacements[115]. Small black circles indicate the location of the pre-Gorkha background seismicity[71].

and anelastic deformation is central to seismotectonics, as it ultimately determines the seismic potential of the MHT and is critical for interpreting the larger-scale evolution[81,82]. Typically, interseismic deformation is interpreted through the lens of interseismic coupling, which is defined as the ratio of the slip rate deficit in the interseismic period to the far-field tectonic shortening rate[83]. The interseismic coupling ratio varies from 0 (for a basal fault that slips aseismically at a rate equal to the plate convergence rate) to 1 (for a fully locked fault). Faults with high coupling values have a high slip rate deficit and will eventually slip to release accumulated strain[81]. As such, interseismic coupling maps can provide information about both fault segmentation and earthquake potential.

Interseismic coupling maps of the Himalaya show that the MHT is largely coupled along its complete length, over a width that varies between 80 and 120 km perpendicular to the arc[71,79,84–88]. The width of the locked-to-creeping transition depends partly on temperature, which affects the fault rheology[81]. As the primary control on temperature is depth, the width of the locked-to-creeping transition, therefore, provides insights into the local dip of the MHT[89]. The line separating the deep creeping part of the fault from the updip coupled region coincides roughly with both the northern edge of microseismicity and the 3,500-m topographic elevation contour[84,90]. However, some recent studies have suggested that the coupling is heterogeneous. For example, a probabilistic estimate derived from a fully Bayesian approach identified four large coupled patches separated by three regions of low coupling[84]. In addition,

per year of convergence at the longitude of Pakistan and 65 mm per year of convergence at the longitude of Bangladesh[73]. More recently, with longer time series and a broader network, the convergence rate between India and Asia has been refined to ~38 mm per year (REFS[76,77]). As half of the convergence is distributed across Tibet, the convergence across the Himalaya is reduced to about ~14–19 mm per year[78]. During the interseismic period, this shortening is accommodated as elastic strain around the base of the MHT, with GPS velocities relative to northern India rising from ~0 mm per year at sites along the MFT, to ~3 mm per year around the Himalayan piedmont, to ~13–17 mm per year north of the High Himalaya[71,79].

Extending the (relatively accessible) observations of interseismic deformation to other parts of the seismic cycle is a challenge. Traditional elastic models assume that interseismic shortening is the mirror image of coseismic deformation[80], but this method does not allow for any net (anelastic) deformation over multiple earthquake cycles[80]. The partitioning between elastic

a detailed GPS velocity solution over Bhutan highlighted local variations in coupling, with a narrower coupled segment in eastern Bhutan and a partially unlocked deeper crustal ramp[88]. Although coupling in some parts of the Himalaya remains poorly constrained because of gaps in GPS observations, local levelling surveys from the Dehra Dun segment[91] (~78° E) suggest that there is no aseismic creep close to the MFT[89]. This indicates that slip on the MFT must occur during another part of the seismic cycle, possibly as a combination of coseismic and post-seismic slip, and earthquakes on the MFT likely reach close to or breach the surface.

Major and great Himalayan earthquakes. There is only a limited number of past great earthquakes, and their along-strike extent has uncertainties. Therefore, and inherently, indicators of seismotectonic segmentation could be alterable in the wake of potential future great earthquakes, whose along-strike extent is not known. Longer ruptures are possible, and scenarios with a larger number of casualties, given enough time, are likely, though undesirable. Therefore, it is important to continue to build our understanding of the distribution and characteristics of past major earthquakes to help inform us of the stress distribution in the crust and, consequently, future seismic hazard assessments.

The MFT and other faults within the Siwaliks have a clear surface expression. Nevertheless, for many years, a lack of observed earthquake-related surface ruptures led to the hypothesis that major Himalayan earthquakes are blind[92]. The 2005 Mw 7.6 Kashmir earthquake, which killed more than 70,000 people, demonstrated that this was not always the case (FIG. 3a). The surface rupture in this event extended over more than ~75 km, with a mean coseismic slip of 4 m (REF.[93]). However, this earthquake cannot be viewed as typical for the Himalaya, as it occurred in the core of the tectonically complex north-western corner of the arc (FIG. 3a).

Since the Kashmir earthquake and the discovery that Himalayan great earthquakes can rupture surface faults[94], the MFT has been the locus of numerous palaeoseismic studies (FIG. 3a). These studies provide constraints on timing (typically based on radiocarbon dates of detrital charcoals, usually correlated to historically documented ground shaking), as well as measurements of local scarps, offset layers and uplifted river terraces. However, palaeoseismic observations might overestimate coseismic slip, as they cannot distinguish between coseismic and post-seismic slip accumulations, or, alternatively, could underestimate coseismic slip, if the slip is distributed across multiple faults. Correlations between multiple palaeoseismic trench data can help assess the lateral extent of ruptures[1,2], but for older events where dating uncertainties are large, miscorrelations could wrongly interpret multiple smaller events as a great earthquake or vice versa[95].

Palaeoseismic data from east central Nepal suggest that a historically undocumented Mw 8+ earthquake in ~1100 AD produced surface slip of 17+5/−3 m and ~8 m of vertical throw, with slip extending for more than 240 km laterally[96–98]. However, other studies have associated the surface ruptures in the area with the 1255 AD Kathmandu earthquake, which killed ~30% of the population of Kathmandu Valley, including King Abhaya Malla, and was, therefore, recorded in historical chronicles[99,100]. Another violent earthquake in 1344 AD in Nepal was associated with a rupture further west between the longitudes of Kathmandu and Pokhara[101].

In western Nepal, the last known great earthquake was the devastating event in 1505 AD (FIG. 3a), sometimes inferred to be as large as Mw 8.7–8.9 (REF.[1]). A palaeoseismic trench in westernmost Nepal suggests that the 1505 earthquake produced ~7.5 m of vertical offset[101,102]. The intervening 500 years have resulted in the accumulation of >10 m of slip deficit along this segment of the MHT, making this one of the most likely sites for the next great earthquake[103]. However, a study of earthquake-triggered turbidites from Rara Lake (western Nepal) reported eight major-to-great earthquakes during the last 800 years, three of which seem to overlap in age with previously reported Mw > 7 events in the region[104].

Since the late nineteenth century, three Mw 8+ instrumental earthquakes have occurred in the Himalayan region: the 1897 Mw 8.2–8.3 Assam–Shillong Plateau earthquake[105,106], the 1934 Mw 8.4 Bihar–Nepal earthquake and the 1950 Mw ~8.5–8.7 Assam earthquake[103,107] (FIG. 3a). In addition to the 2005 Mw 7.6 Kashmir earthquake[93], a number of recent earthquakes have also been quite destructive, including the 1905 Mw ~7.8 Kangra earthquake[108] and the most recent 2015 Mw 7.8 Gorkha earthquake[109,110].

The 2015 Mw 7.8 Gorkha earthquake. The most recent major earthquake in the Himalaya occurred on April 25, 2015, when a Mw 7.8 earthquake struck central Nepal[109,110]. This event was followed by a series of Mw > 6 aftershocks[61,111,112] and triggered a Mw 7.3 event to the east 17 days later[113,114] (FIG. 3b). The Gorkha event is the most recent major earthquake in the Himalaya and the best instrumented in the region. The earthquake caused devastation in the Gorkha region; however, the data from this event offer a unique opportunity to investigate how coseismic and post-seismic deformation relate to tectonic structures in the Himalaya, and can help inform future earthquake hazard assessment.

The datasets provided by the 2015 Mw 7.8 Gorkha earthquake offer a window into seismic rupture processes and large-scale crustal deformation at unprecedented spatial and temporal resolution. Notably, the Gorkha earthquake is the first example of a large continental megathrust rupture beneath a high-rate (5-Hz) GPS network[110] (FIG. 3b). Through the combined use of GPS and satellite (Interferometric Synthetic Aperture Radar, InSAR) data, it is possible to characterize the rupture process as a ~20-km-wide slip pulse lasting ~6 s, with peak sliding velocity of 1.1 m s⁻¹. The records indicate an eastward propagation at ~3.3 km s⁻¹ over a ~140-km distance[110]. The smooth onset of the slip pulse excited a resonance of the Kathmandu basin with a period of 4–5 s, causing collapse of some tall structures, including cultural artefacts, but leaving smaller buildings generally intact[110]. Geodetic measurements and satellite data constrain surface motions during the earthquake[109,113,115–117], revealing uplift of about 1.5 m in

the Kathmandu basin[113], with subsidence of the High Himalaya further north by about 0.6 m (REF.[117]) (FIG. 3b).

The main shock and the first months of aftershock activity provided an outstanding opportunity to document the relations between the MHT, regional tectonic structures and seismicity[54,61,117–119]. Furthermore, six weeks after the earthquake, a dense seismic network (called NAMASTE, standing for Nepal Array Measuring Aftershock Seismicity Trailing Earthquake[120]) was deployed in central Nepal. In approximately 11 months, this seismic network identified >8,000 earthquakes, helping to further decipher the relationship between the aftershocks and tectonic structures at depth[63], and the lateral variations in both[62,112]. Overall, these data are best explained by a gently dipping fault at depths between 10 and 15 km and continuing downdip on the steeper mid-crustal ramp[54,117,118]. The presence of this ramp has important implications for both the Himalayan seismic cycle[121] and long-term construction of the Himalaya[117,122].

GPS records of surface motions in the months immediately following the earthquake showed that >70 mm of afterslip occurred locally, north of the rupture[123,124]. However, the MHT south of the rupture patch has remained coupled[123,124], indicating that substantial elastic strain must be present at the updip limit of the 2015 rupture. Given that the Gorkha earthquake occurred in the same location as a similar-magnitude earthquake in 1833, these observations suggest that major blind earthquakes can re-rupture fault patches, whereas great earthquakes might propagate to the surface, driven by residual strain accumulated over centuries[89,121,125]. Further advances in understanding the seismic behaviour of the MHT will come from combining the existing and rapidly increasing streams of seismic, geodetic and geologic data with new constraints from inevitable future earthquakes.

Transient versus permanent deformation

The rise of Himalayan topography involves long-term crustal shortening and uplift. In addition, earthquake-related processes, which are generally transient phenomena, can also contribute to the building of topography via inelastic strain accumulation. However, the spatiotemporal relationship between permanent and transient deformation is still poorly constrained. In this section, we reconcile observations from both long-term and short-term deformation processes to synthesize the current understanding of how the MHT operates in space and time, and discuss the processes by which mountains grow.

Role of the mid-crustal ramp. The presence of a mid-crustal ramp connecting the flat décollement under the Lesser Himalaya with the deeper décollement under the High Himalaya has been supported by results from structural geology[118], microseismicity[126], seismic reflection[46], magnetotelluric sounding[48], geodetic data[73,122] and uplift rates[65]. Slip on this ramp (and previous manifestations of the ramp) has led to the development a large anticlinorium that forms the backbone of the Himalaya (in Nepal, this is called the Gorkha-Pokhara Anticlinorium, or GPA; FIG. 2).

This ramp is one of most prominent structural features linked to both long-term tectonic and short-term seismic processes, although its position has stepped forward (southward) several times over the last 15 Ma, in a process described variously as duplexing, accretion and tectonic underplating (FIG. 4). This, together with frontal accretion through break forward of the MFT (and, prior to that, of the MBT and MCT), has been the dominant process contributing to volume growth of the Himalayan wedge since the Middle Miocene[43,127]. Furthermore, physics-based numerical models[128], analogue models[129] and geologically informed structural cross sections[118] indicate that the flat–ramp–flat geometry of the MHT causes long-term topographic growth localized above the ramp[43,122,130] (FIG. 4a,b).

At shorter timescales, major and great earthquakes rupture part or all of the megathrust and incrementally contribute to the evolution of the topography[117]. These episodic ruptures, which last a few tens to hundreds of seconds, are followed by a post-seismic adjustment period (for example, afterslip and viscoelastic relaxation)[81] with accelerated creep rates and increased seismic hazard. This creep decays over the course of weeks to months to years back to interseismic conditions, during which stress builds up at the border between the locked and stably creeping (aseismic) parts of the MHT (FIG. 4c). During these interseismic periods, micro to moderate earthquakes (Mw < 6) record the accumulation of stress around the transition zone[126]. Seismological networks record thousands of these events every year along the Himalayan range (FIG. 4d), occurring mostly in a broad cloud at mid-crustal depths below the front of the high topography[126], with some events extending into the deep crustal root and the upper mantle[131,132]. In some regions, this seismicity can be resolved as clusters localized along and above the MHT décollement, along the mid-crustal ramp or at contacts between Lesser Himalayan duplexed rocks[60], demonstrating that seismicity is at least partially controlled by structural heterogeneities (FIG. 4d). An increase in event frequency during the winter months demonstrates that broad stress changes associated with the Indian monsoon are able to modify the stress state below the Himalaya[133]. Temporal patterns like this can provide an opportunity to constrain the absolute stress state.

The interseismic microseismicity is a response to the strain accumulating in the crust, as ~14–19 mm per year of viscous creep on the deepest part of the fault decreases to zero slip on the coupled part of the fault across a 20–25-km large transition zone[71,78,84,88,134] (FIG. 4c). During the interseismic period, this process is accommodated by elastic shortening of the crust and results in peak uplift of 7–8 mm per year (REFS[71,122,130,134]). The downdip limit of the locked fault falls in the vicinity of the 350 °C isotherm[71,127], a temperature that controls the transition to stable sliding in quartzo-feldspathic rocks[135,136], and is also spatially correlated with the base of the mid-crustal ramp[134], suggesting that the ramp development is likely partly thermally controlled.

The mid-crustal ramp affects not just the interseismic period but also coseismic rupture segmentation and rupture characteristics. Several observations suggest that

---

Blind earthquakes
Earthquakes where fault slip does not reach the Earth's surface and, hence, do not produce a fault scarp.

Accretion
Process by which material from the lower (subducting) plate is removed and added to the upper plate by tectonic processes, such as imbricate thrusting and/or folding and thrusting.

the width of the locked–creeping transition could be an important determinant for the nucleation of major and great Himalayan earthquakes[89]. Where the downdip width of the transition is narrow (~20–25 km), major earthquakes are observed to occur at intervals of a few hundred years. Conversely, where the transition zone is wider, great earthquakes occur at long time intervals (millennia)[89]. Also, seismic analyses following the Gorkha main shock reveal that several patches slipped sequentially[109,116,137], with the downdip slip region characterized by a larger ratio of high-frequency (0.03–0.2-Hz) to low-frequency energy compared with shallower areas[138]. This high-frequency energy radiation might be associated with heterogeneous prestress[139] or might be related to the transition from the more steeply dipping mid-crustal ramp onto a more gently dipping, smoother, stratigraphically bounded décollement[118] (FIG. 4b). The updip slip patch exhibited relatively continuous rupture, whereas the downdip rupture cascaded along the

fault[138], suggesting that the fault geometry affected the rupture propagation and energy frequencies[116,118], possibly associated with a damage zone produced by the fault bend[117,122].

Line-of-sight displacement of the Mw 7.3 Gorkha aftershock indicates a similar but more compact pattern compared with the displacement from the main shock[113]. The displacement occurred near the eastern edge of the main rupture, suggesting that it might have been triggered by a Coulomb stress concentration from the main shock[110]. Thousands of aftershocks were generated at the periphery of these two ruptures, mainly in the hanging wall of the MHT[61,111,112,120], with seismic clusters and associated focal mechanisms revealing the steeper ramps bordering the main shock slip patch[140]. It appears that seismic and geodetic activity across the earthquake cycle is affected by the long-term geological structure. This could be useful for hazard assessment, as geological mapping and observations during the interseismic period can
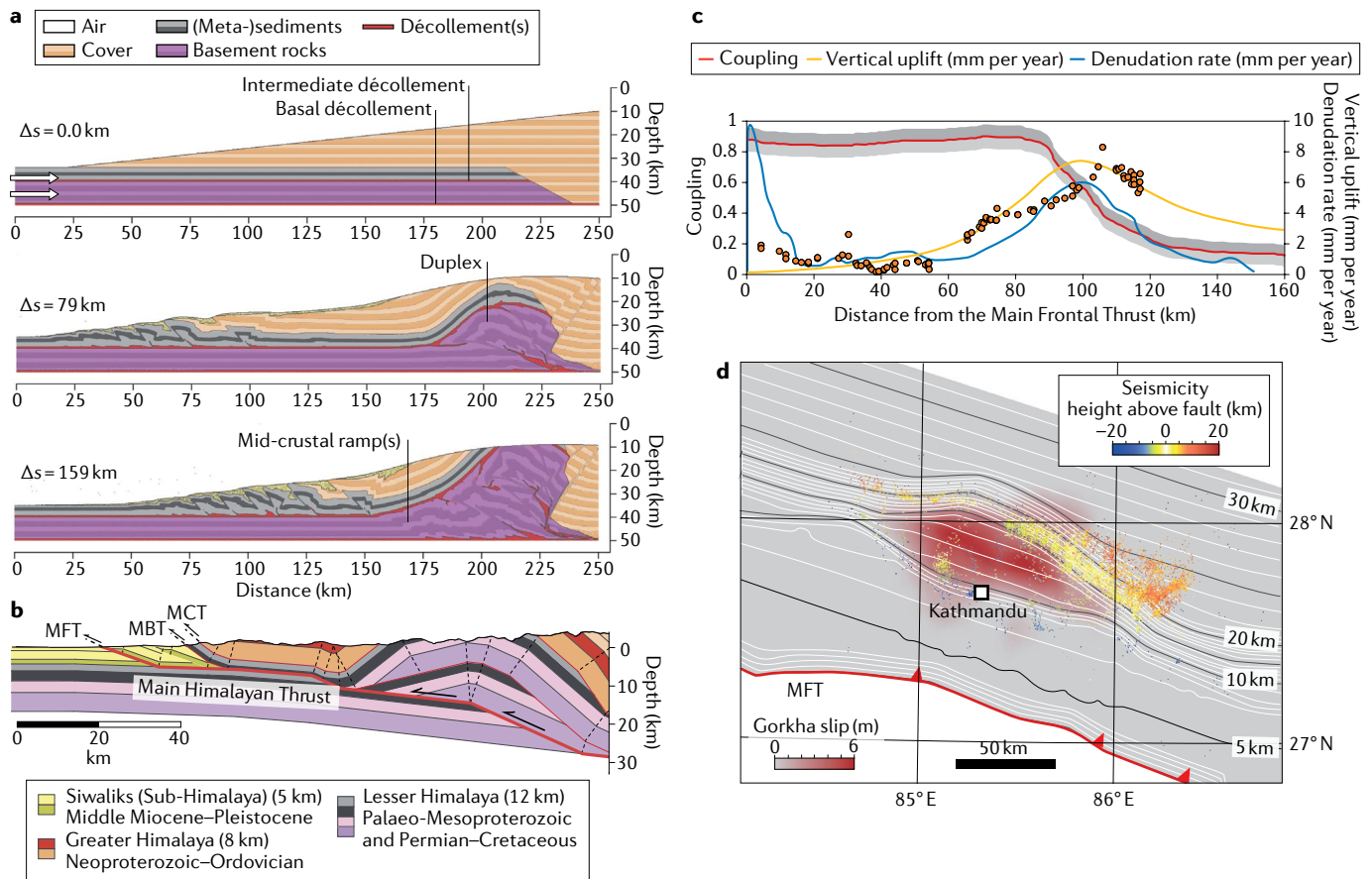

Fig. 4 | **Crustal-scale duplexing and seismic behaviour of the mid-crustal ramp. a** | Three temporal snapshots from a sandbox-like physics-based numerical model, showing how the presence of two décollement levels and the coupling between deformation and erosion determine the occurrence of underplating, crustal-scale duplexing and antiformal stacking[128]. **b** | A new balanced cross section of the present-day central Nepal Himalaya based on constraints from surface geology and the 2015 Gorkha earthquake[118], showing the duplex structure and the geometry of main faults at depth. MBT, Main Boundary Thrust; MCT, Main Central Thrust; MFT, Main Frontal Thrust. **c** | Comparison between interseismic coupling[84] (solid red line with uncertainties in grey) and interseismic uplift rate from

levelling measurements[130] (orange circles) and synthetic data[121] (solid orange line), and long-term denudation rate[65] (solid blue line). **d** | Map view of the Main Himalayan Thrust in central and eastern Nepal[118], and aftershocks (between latest June 2015 and mid-May 2016) following the 2015 Mw 7.8 Gorkha earthquake[63]. Contours show depth to thrust surface. Red area shows slip amounts during the Gorkha earthquake. Coloured dots indicate the location of aftershocks relative to the depth of the Main Himalayan Thrust. Panel **a** adapted with permission from REF.[128], Wiley ©2020. American Geophysical Union. All Rights Reserved. Panel **b** adapted with permission from REF.[118], CC BY 4.0 (https://creativecommons.org/licenses/by/4.0/).

be tested against each other, and, together, they can provide a basis for forecasts of future earthquake locations, limits and rupture characteristics[60–63,118] (FIG. 4d).

Along-strike and downdip segmentation. Based on the along-strike continuity of the main geological units, the Himalaya are often considered cylindrical[32,141] and tectonic models for orogenic growth have largely focused on cross-orogen sections. Nevertheless, notable along-strike variations in both the downgoing Indian Plate and the respective upper plate have been reliably documented (FIG. 1b). Furthermore, lateral variations in the subducting slab must affect the flexural geometry and tectonic stresses across the lithosphere, and should be taken into account in tectonic models of orogenic growth.

The topography is one of the clearest indicators of along-strike variation, pointing to a prominent boundary at about 90° E; this location coincides with a change in the curvature of the arc[142]. This boundary is also the confluence of the deeper and thicker Ganges foreland basin and the very shallow Brahmaputra foreland basin[143] (FIG. 5). East of this boundary, the Shillong Plateau and Assam Valley, pinched between the eastern Himalaya and the Indo-Burma ranges, likely play a key role in shaping the seismotectonics of the area[144] (FIG. 1b), as expressed by the active seismicity in the Brahmaputra foreland (FIG. 5b). Cross-orogen topographic profiles further highlight the difference between the relatively lower-lying foothills in Nepal (where the MFT lies ~10–30 km south of the MBT, so the frontal range is made up of relatively young Siwalik sediments) and the steeper front in Bhutan (where the MFT and the MBT are tightly spaced, and the range is composed of the much older and stronger Lesser Himalayan sequence)[145]. In addition, prominent >8,000-m peaks are located mostly in the central Himalaya (FIG. 5a), as well as in the western syntaxis, and are absent in both the eastern and the western Himalaya.

Further evidence of potential segmentation can be seen to the north, in southern Tibet, where a series of rifts accommodate east–west extension[146]. These rifts span from a few to several hundred kilometres from north to south, and some reach the High Himalaya and connect to prominent, deeply incised valleys dissecting the orogen (FIG. 5a), such as the Kali Gandaki and the Sikkim half window. These valleys are apparent markers of Himalayan segmentation at the surface, though it remains unclear whether these are caused by downgoing Indian basement highs, by duplex formation or by the southward propagation of South Tibetan extensional grabens (FIG. 5a).

A number of tectonic features inferred from surface observations have been previously proposed to cut across the orogen, referred to as "lineaments"[147,148]. Many of these lineaments could not be identified or confirmed by later studies, and some even cross each other in a dynamically unsustainable way[148]. Nevertheless, there are three north–south trending crustal fault systems within the Himalaya that divide the orogen into different tectonic segments from east to west. These fault zones span considerable length and could play a role in segmenting seismotectonic behaviour: the Western

Nepal Fault System, the Dhubri–Chungthang fault zone and the Kopili fault zone (FIG. 5a). The Western Nepal Fault System cuts across the Himalaya at 82–83.5° E and is proposed to accommodate strain partitioning[149], but shows no particular instrumental seismicity. The Dhubri–Chungthang fault zone has been identified by an alignment of mid-crustal to lower-crustal earthquakes; this is likely a primary basement structure that allows dextral motion between the north-west corner of the Shillong Plateau and north-west Sikkim[150]. West of the Dhubri–Chungthang fault zone, seismicity in the Himalaya is dominantly thrust sense, whereas the foreland is largely aseismic. However, to the east, there is marked strike-slip activity with clear seismicity in the foreland (FIG. 5b). The Kopili fault zone, on the eastern edge of the Shillong Plateau and extending beneath the eastern Bhutan Himalaya, exhibits a broadly linear distribution of earthquakes[151]. Ongoing dextral deformation within both the Dhubri–Chungthang fault zone and the Kopili fault zone is compatible with surface deformation observed by GPS[152,153]. The Dhubri–Chungthang fault zone and the Kopili fault zone are thought to represent block boundaries, and the two resulting terrains rotate clockwise with respect to India[152].

The deep structure of the incoming India Plate likely also influences Himalayan segmentation, through inherited subsurface ridges. The Delhi–Haridwar, Faizabad and Munger–Saharsa ridges (FIG. 5a) are broad basement highs that can be identified in the depth of the sedimentary basin[142,143] (FIG. 5a). These ridges have been proposed to act as barriers to rupture propagation during major Himalayan earthquakes[154], as they could alter the geometry and strength of the MHT as they subduct. The Faizabad ridge is not documented to extend to the Himalayan front, but the two other ridges do seem to reach the front in the form of subsurface faults[155] (FIG. 5a). The Delhi–Haridwar ridge is localized and aligns with the Mahendragarh–Dehradun fault, which shows some seismicity (FIG. 5b). The Munger–Saharsa ridge is bounded by a system of tear faults at a high angle to the orogen[155], the easternmost of which (the Malda–Kishanganj fault) terminates the deeper part of the Ganges foreland basin[143,154] (FIG. 5a).

Flexure of the entire Indian lithosphere exerts a deeper control on Himalayan segmentation. As the plate bends beneath the orogen, its flexural geometry can be mapped by gravimetry[156,157] and verified by numerical modelling[158] and structural seismology[159]. Gravity data, mostly along 2D orogen-perpendicular profiles[160–163], filled in by targeted surveying of data gaps[164,165], has allowed the community to infer that plate rigidity is fairly homogeneous along the Nepal Himalaya[164], but flexure occurs on a shorter wavelength in the Bhutan Himalaya[165]. Gravity anomaly residuals with respect to the average cross-orogen flexural profile (arc-parallel gravity anomalies, or APaGAs) reveal four main segments along the Himalaya, with alternating signatures[142] (FIG. 5a), the boundaries of which correlate with shallower structural features: the Mahendragarh–Dehradun fault, the Malda–Kishanganj fault and the Kopili fault zone (FIG. 5a). Moreover, these three segment boundaries coincide with the lateral rupture extents of major
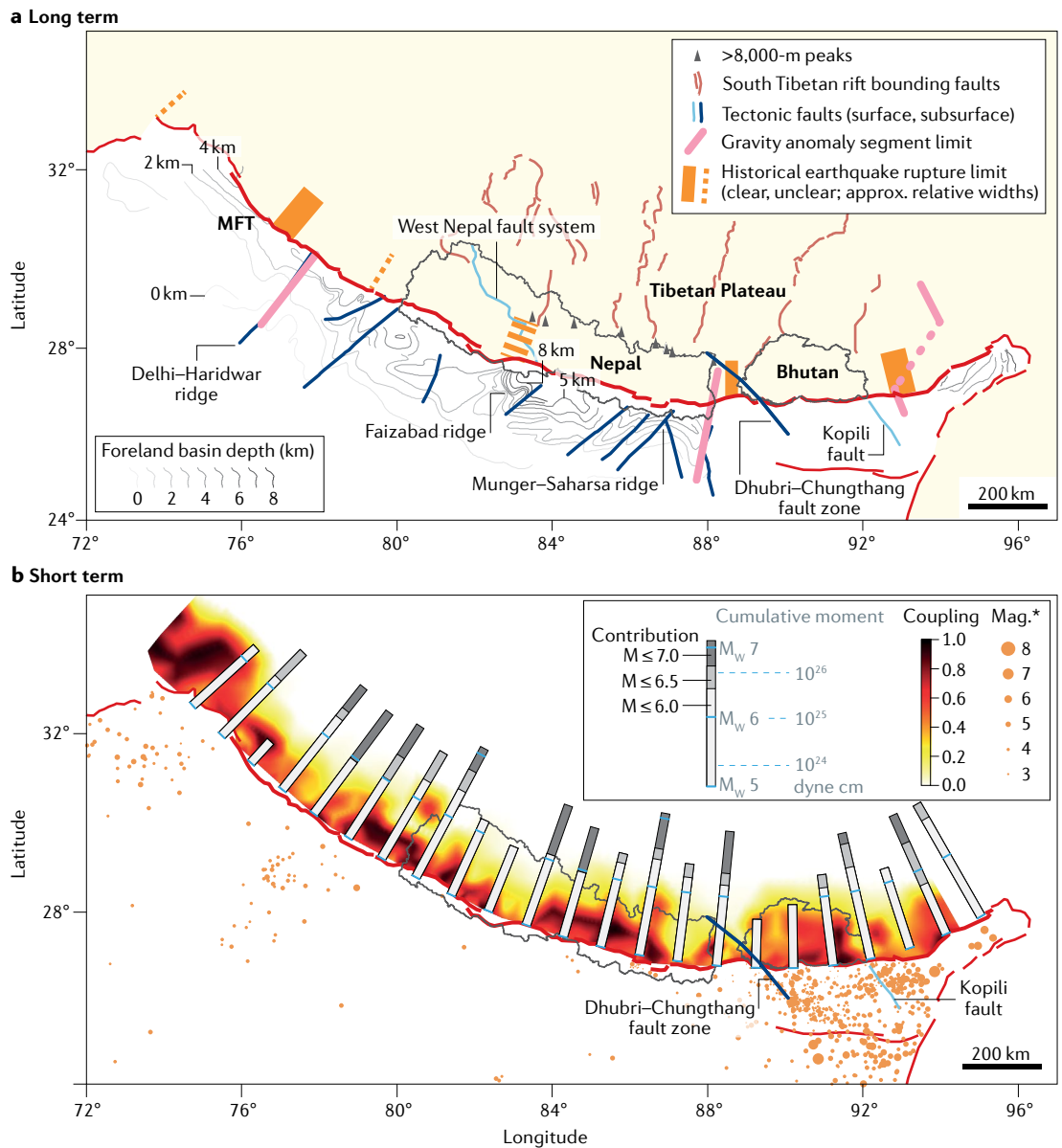
a Long term

b Short term

Fig. 5 | **Segmentation indicators of the Himalaya. a** | Long-term indicators include tectonic faults, basement structures, gravity anomaly segments and historical earthquake ruptures. Deforming orogenic area is shaded in pale yellow. Foreland basin depth contours, inferred ridges and inferred faults from REF.[143]. Active surface and subsurface faults are shown in light and dark blue, respectively. South Tibetan rift zones are shown as light red lines[146]. Large-scale structural segments delineated by arc-parallel gravity anomaly residuals are in pink[142]. Rupture area limits of all Mw ≥ 7.5 earthquakes since 1500 AD are in orange[142]. Nepal and Bhutan's borders are shown in black for reference. **b** | Short-term indicators include seismicity and interseismic coupling. Cumulative seismic moment (NEIC catalogue from 1905 to May 2020) of selected earthquakes, expressed as equivalent energy and earthquake magnitude, with bars shown at 100-km segments along the Main Frontal Thrust (MFT). Magnitude selections (≤6.0, ≤6.5, ≤7.0) reflect realistic levels of catalogue completeness[142]. Posterior mean coupling model obtained from Bayesian inversion of geodetic data[84], accounting for data uncertainties and 10% of prediction uncertainties. Earthquakes in the foreland (from the NEIC, as well as accessible temporary network catalogues[150,212]) are shown as orange dots. The active frontal thrusts are shown in darker red, with the MFT shown as the thicker red line.

and great Himalayan earthquakes[142] (FIG. 5a), suggesting that these long-lived features could influence transient seismic behaviour.

These segment boundaries might also alter interseismic behaviour. Bayesian modelling of interseismic coupling on the MHT points to similar segment boundary locations as those identified from APaGAs (FIG. 5b), with

a possible additional segment boundary at the Faizabad ridge[84]. A similar pattern emerges from the distribution of cumulative seismic moment of instrumental earthquakes in the Himalaya, with relative lows at these locations, including the Faizabad ridge[142] (FIG. 5b). The Faizabad ridge might, therefore, affect the segmentation of the MHT, but is apparently not related to plate

flexure[164] or APaGAs[142]. Other segment boundaries have likely developed during orogeny, such as ramps and related pinch points and tear faults, which might arrest or affect rupture propagation, owing to variations in fault stress, friction and fluids, like in the Gorkha earthquake[61,118]. These observations together suggest that it might be possible to better constrain future seismic hazard through the identification of long-lived tectonic features, supported by interseismic observations.

Long-term topographic growth. The Himalaya are particularly striking because of the characteristic high and rugged topography, which includes ten of the world's 14 highest peaks. This topography has evolved over the ~50-Myr collisional history of the range, with extensive tectonic shortening both within and across the margins of the Tibetan Plateau[166–169] (FIG. 1). Across the Himalaya, this shortening history can be reconstructed using geological cross sections, but, owing to erosion and an inability to quantify penetrative strain, the resulting estimates are minima, and have a wide range from 70 to over 900 km (REFS[118,170–174]). These variations are often related to the study location, but are likely influenced by assumptions about the style of deformation. For example, some research groups tend to focus field efforts within national borders, owing to permit requirements and collaborative networks, and, therefore, structural style assumptions by different groups could be wrongly interpreted as structural changes along strike. Plate circuit reconstructions that incorporate palaeomagnetic constraints provide more complete estimates, and indicate between 900 and 1,500 km of shortening across the Himalaya[167,171].

Geochemical and fossil plant proxies suggest that the Himalaya reached ~2,300 m elevation by the beginning of the Miocene and at least ~5,500 m by ~15 Ma (REF.[175]). Stable isotope palaeoaltimetry estimates based on oxygen in carbonate precipitated from surface water suggest that the Himalaya were at elevations close to the present day by the early Miocene[176]. Hydrogen isotope ratios of hydrous minerals in the South Tibetan Detachment shear zone record the meteoric water composition and indicate that the central Himalaya reached an elevation around ~4,500–6,000 m by the late Early Miocene[177]. These proxies generally show that the collision began at ~50 Ma, whereas substantial topographic growth did not begin until ~20 million years later[175–177]. The more intensive metamorphic and magmatic activity in the Himalaya since 23 Ma corroborates this timing[178].

Neither the current topography nor the geodetically inferred uplift rate is a record of the modern net uplift rate. One reason for this discrepancy is attributed to erosion, a fundamental mechanism influencing mass redistribution at the surface[7,8,179–181]. The pattern of fluvial incision in central Nepal indicates values up to 10–15 mm per year in the Sub-Himalaya, dropping to 0.5–1.5 mm per year across the Lesser Himalaya, then rising again to 4–8 mm per year across the High Himalaya[65]. The thermal and tectonic evolution of the crust beneath the Himalayan range also influences the net uplift rate, which evolves through time as faults break forward[17,127,182]. Thermometric and thermochronological

methods (mostly from ^{39}Ar/^{40}Ar ages of muscovite), combined with structural geology, indicate that the Lesser Himalaya has been exhumed at an average rate of 5 mm per year[182]. These results suggest that, since the mid-Miocene, the Himalayan wedge has mainly grown by overthrusting and tectonic underplating, rather than by frontal accretion[182].

Furthermore, cosmogenic ^{10}Be concentrations in river sediments were used to quantify catchment-scale denudation at the 100–1,000-year timescale[179]. Rock-uplift values derived from river-profile analysis[65] are notably higher than the ^{10}Be-based denudation rates[179]; however, their spatial patterns are similar. These results indicate that the apparent correlation between denudation and uplift rate is primarily controlled by tectonic processes, whereas precipitation yields only a second-order contribution[179]. Mapping fault geometries can provide predictions for net topographic growth. Uplifted river terraces suggest that, over thousands of years, most or all geodetically observed shortening reaches the surface on the MFT, with minor slip on out-of-sequence thrusts[64,68]. As the same net slip is accommodated over the full MHT, we expect higher long-term uplift rates where the slope MHT dips more steeply[118,182] (FIG. 6).

However, the downdip geometry of the basal MHT remains contested. Although based primarily on geological reconstructions, most researchers agree that the orientation of the MHT varies downdip[33,118,126,183–185]. The base of the MHT mid-crustal ramp lies at ~15–30 km below sea level, flattens onto a shallowly dipping bed-parallel décollement at ~10–15 km below sea level for ~100 km and rises to the surface on the more steeply dipping MFT, with additional, internal ramps linking different stratigraphic levels[33,69,118]. Variations in fault dip are likely important for seismic processes, and, although some can be constrained with imaging[45,46,54,69,117,140,186], others are likely below the resolution of imaging techniques.

Between the MFT and the High Himalaya, the topography is likely more heavily dominated by inherited topographic growth from past shortening (moderated by erosional processes and lithology), rather than modern fault slip. For instance, rocks in the hanging wall of the MBT (which is considered, at most, minimally active) form the low Mahabharat mountain range, most likely owing to their stronger lithology compared with the much younger and softer Siwaliks sediments to the south[65]. Within the Siwaliks themselves, the more rugged topography is associated with exposures of the Lower Siwaliks, which have been more deeply buried and consolidated, despite the fact that these often sit above older, less active thrusts to the north[34].

Our synthesis indicates that observations of erosion, or other records of tectonic growth over thousands of years, are likely a good source for constraints on the locations and orientations of active faults, as they integrate the cumulative contribution over multiple earthquake cycles, but are less affected by inherited topography.

Topography and the seismic cycle. Unlike erosion rates, which average across the seismic cycle, direct observations of uplift primarily capture specific windows during the interseismic, coseismic and post-seismic periods.
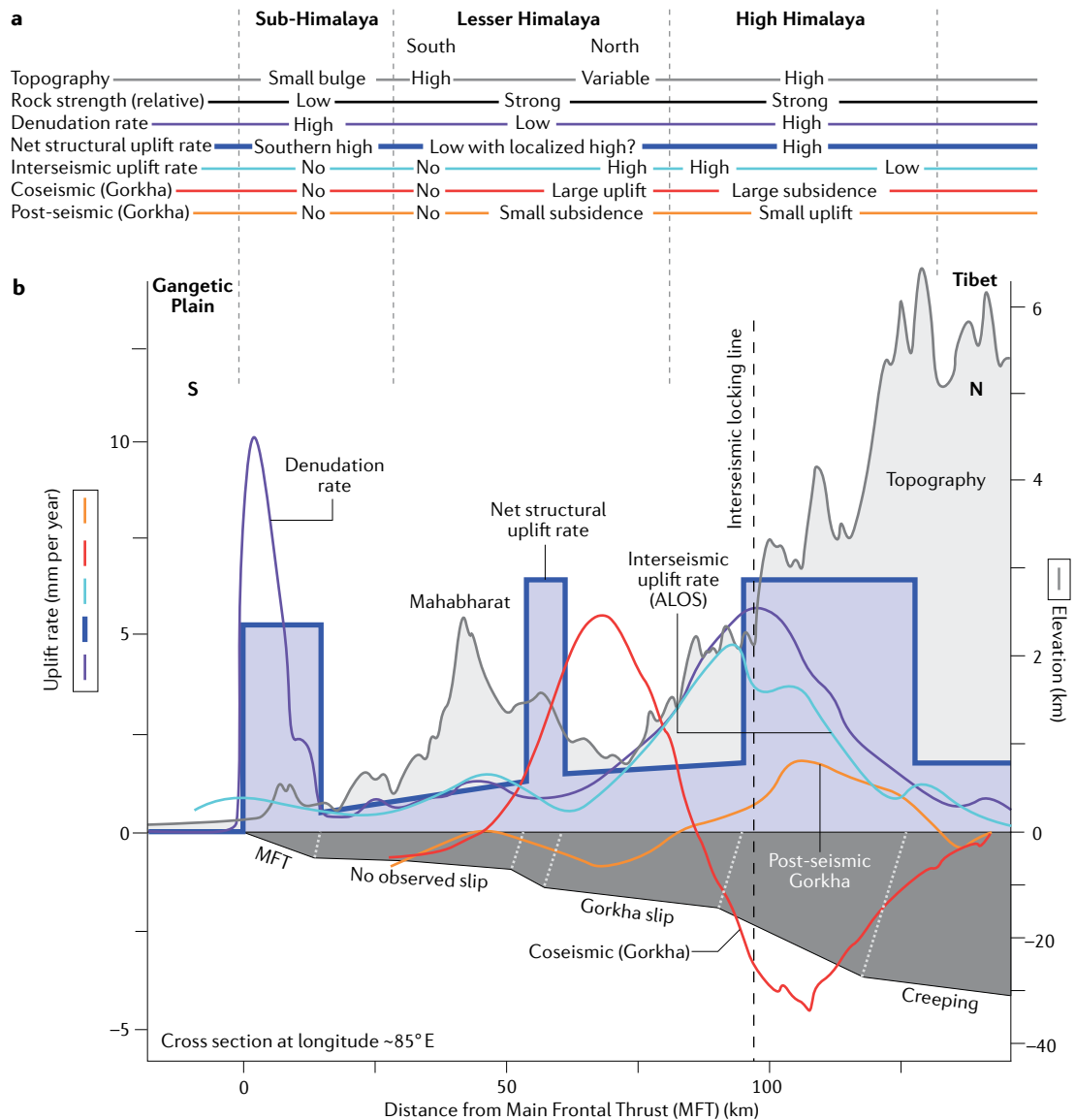
Fig. 6 | **Cross section across central Nepal showing different proxies for uplift rate. a** | Divisions of the Himalaya and their characteristics. Rock strength description is broadly defined for the Siwaliks versus the Lesser and Greater Himalayan sequences[65]. **b** | Cross section (longitude ~85° E) showing topography, interseismic uplift rate from ALOS InSAR[86], coseismic uplift in Gorkha[213], post-seismic uplift following Gorkha[213], denudation rate[122], net structural uplift rate inferred from the geometry of the Main Himalayan Thrust (MHT) with a constant slip rate of 15 mm per year on the basal fault, interseismic locking line representing transition from deep creep to shallow locking (black dashed line)[134], and the MHT and its hanging wall (dark grey shading)[118]. Coseismic and post-seismic uplift amounts are converted to rates by assuming that the typical rupture behaviour in this region is represented by the 1833 and 2015 earthquakes, and that these events were identical[118]; therefore, the rates are simply measurements from Gorkha divided by 182 years. The measured post-seismic uplift[86] ends on July 22 2015; we assume that this period captures half of the total post-seismic uplift, so the rate presented here is twice the measured displacement divided by 182 years. Note that the sum of the interseismic, coseismic and post-seismic curves would not equal the net uplift, because the Gorkha earthquake did not rupture the frontal part of the MHT.

These seismic cycle variations reflect a combination of transient, elastic strain and permanent, inelastic strain, and each part of the seismic cycle has a different distribution of deformation[80,81]. As a consequence, the observed uplift patterns often look nothing alike, although they should eventually sum to produce the net uplift described in the previous section.

During earthquakes, surface uplift depends on the local fault dip, the distribution of slip and the bulk Poisson's ratio of the rocks[187] (FIG. 6). The 2015 Gorkha earthquake, which is, by far, the best documented earthquake in the Himalaya, caused maximum surface uplift of ~1.5 m, roughly correlating with the slip patch. This is matched by a region to the north that subsided ~0.6 m, representing the release of interseismic elastic strain[113,114,117,188]. As this event was a partial rupture of the MHT, the coseismic uplift pattern should not be expected to correlate with the net uplift, and, indeed, it

Interseismic locking
A mechanical term referring to the response of a fault to applied stress during the interseismic period. A fault that is frictionally locked does not slip, despite the application of stress.

does not (FIG. 6). Surprisingly, although there has been continued post-seismic creep within both the coseismic rupture patch and the downdip (with an uplift pattern that is approximately the opposite of the coseismic, with lower amplitude), creep in the newly stressed area updip of the rupture patch has been minimal (<10 mm)[189]. This indicates that the updip region must slip (and, therefore, experience topographic change) during some other part of the seismic cycle, likely associated with updip coseismic slip[57].

The interseismic uplift rate, which can be inferred along the whole arc, records elastic strain accumulation above the downdip boundary of interseismic locking, and is distinctly different from the net uplift expected across multiple earthquake cycles (FIG. 6). Interseismic uplift rates can be directly measured from InSAR[122], levelling measurements[130] or inverted from interseismic horizontal GPS measurements[134].

Coseismic and post-seismic uplift patterns have the potential to inform us about details in fault geometry, but interpretations are not straightforward. Some researchers have suggested that the geodetic deformation produced by the 2015 Gorkha earthquake is not consistent with a mid-crustal ramp, and, instead, suggest a planar MHT[119]. However, the proposed planar MHT geometry is unable to explain the exposed geology[118], and more recent inversions of the Gorkha coseismic, aftershock and post-seismic geodetic deformation show that this dataset alone cannot discriminate between geometries with and without a downdip ramp[190].

Evidence for the deep ramp instead relies primarily on the observation of a 50-km-wide anticlinorium and associated topography[32], where deep rocks have been raised to the surface (documented by thermochronometry[182]). This ramp also generally correlates with geophysical data that indicate the accumulation of interseismic strain[84,134], such as microseismicity patterns[71,126], association with the lower edge of the coseismic slip from the 2015 Gorkha earthquake[118] and steeper aftershock focal mechanisms following the earthquake[140].

The intermediate ramps between the MFT and the downdip ramp are more difficult to observe from interseismic strain accumulation, as they lie in the stress shadow of the locked downdip part of the fault[83]. These blind ramps are largely inferred based on geological mapping of folding patterns and stratigraphy, although in the Gorkha region, a blind ramp correlates with the updip edge of coseismic slip[118] and steeper aftershock focal mechanisms[140], similar to the downdip edge.

Near the toe of the system, the more steeply dipping MFT has not been observed to slip during the instrumental period, and no seismic cycle observations point to deformation in this region. However, this fault can be directly mapped at the surface, and its subsurface extent can be imaged with high-resolution seismic reflection profiles, as it lies within the upper few kilometres[69]. The MFT is, therefore, well constrained, although it can feature near-surface dip variations[191].

It has been proposed that some of the interseismic uplift around the High Himalaya is not recovered elastically but, rather, becomes permanent strain[73,78,84,192]. Certainly, the geology is consistent with extensive off-fault deformation associated with folding. However, it is unclear globally how hanging-wall folding is accommodated across the seismic cycle. Coseismic folding has been observed in some earthquakes (for example, 1999 Chi-Chi, Taiwan, REF.[193]), whereas in other cases, folds grow interseismically (such as in south-western Taiwan, REF.[194]). Geological[195] and numerical models[121,128] could prove useful for increasing our understanding of the mechanisms of off-fault deformation and shortening in the future, for both the downdip Himalayan ramp and elsewhere. Understanding the partitioning of uplift into elastic and inelastic components could help to forecast deformation in parts of the earthquake cycle that are not observable owing to a lack of earthquakes, with the ultimate goal of understanding how seismic cycle processes sum to produce the net deformation.

Summary and future perspectives

This Review highlights the key elements of long-term tectonic and short-term seismic processes in the Himalayan region. We discuss the interplay between transient and permanent deformation that has resulted in the building of Himalayan topography. Better understanding of the various modes of interaction are crucial, as they affect short-term deformation, structural segmentation and, eventually, the long-term growth of the Himalayan orogen. Multidisciplinary efforts have provided important constraints on the links between the seismic cycle and topography, but also highlight areas that need further, joint multi-approach investigations (FIG. 7).

Conclusions. The presence of inherited tectonic structures seems to affect the segmentation of the Himalayan arc. However, whether this segmentation is persistent at all timescales remains unclear. The Gorkha earthquake provided insights into ground motion frequencies, rupture directivity and fault geometry influence, but we do not yet know whether these characteristics represent broad behaviour patterns. Answering such questions might not be possible until there are more observations of earthquakes on well-instrumented faults.

Evidence from limited past and historical earthquakes suggest that only great earthquakes (Mw 8+) might be capable of rupturing up to the megathrust front. Major Mw 7+ earthquakes, which can still cause large-scale devastation and are documented in historical chronicles, are often only associated with partial ruptures of the MHT at depth. Palaeoseismic records excavated at the front of the range (FIG. 3a) are, so far, limited to a few infrequent great earthquakes, and even these records are often limited by the variability in the quality of preservation of the surface ruptures[196]. Palaeoliquefaction investigations[197] and earthquake-triggered turbidites[104] from Rara Lake (western Nepal) have shown that alternative evidence can be found for smaller events that did not rupture the surface; studies like this could provide further insights into the slip deficit and the expected seismicity pattern. However, many open questions remain regarding the magnitudes, recurrence intervals and styles of earthquakes on the MHT, and how they relate to the long-term building of topography in the Himalaya. In particular, given the lack of instrumental observation
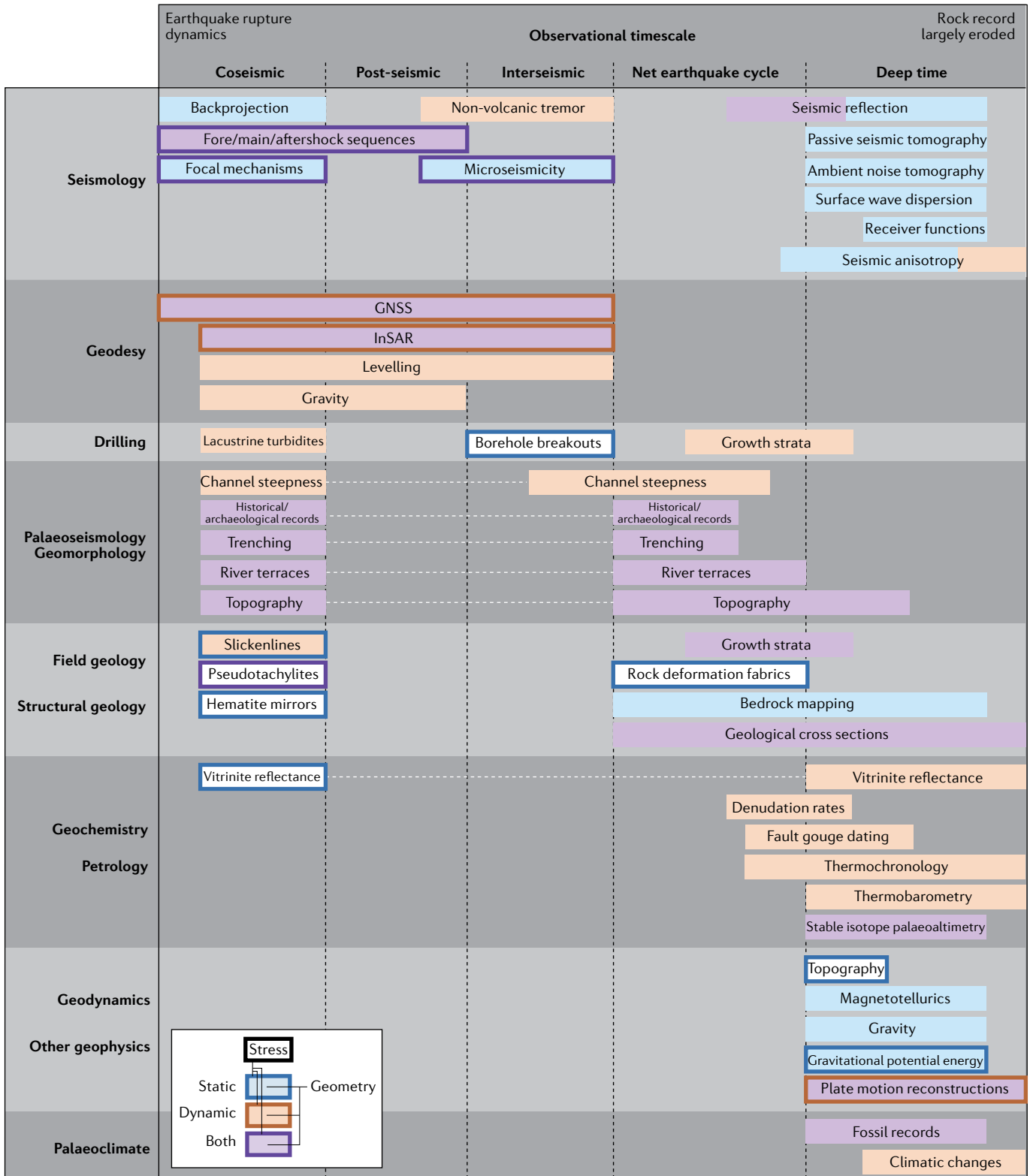
Fig. 7 | **Datasets that illuminate the tectonics of the Himalaya.** Datasets are classified by subfield (vertical axis) and observational timescale (horizontal axis). Colours represent the type of information that can be learned either by direct observation or by the use of the datasets in models. Solid colours show geometrical information (blue = static geometry, orange = dynamic change in geometry, purple = both) and borders show information about the stress field (blue = static, orange = dynamic change in stress, purple = both). Note that each subfield can only observe part of the timescale and, therefore, a complete understanding of Himalayan tectonics requires a multidisciplinary effort aimed at finding new methods of observation and stretching the bounds of existing techniques. GNSS, Global Navigation Satellite System; InSAR, Interferometric Synthetic Aperture Radar.

of surface rupture on the MFT, we do not know how much of the slip observed palaeoseismically at the surface occurs coseismically versus post-seismically, nor do we know whether slip on such a shallow fault can radiate ground shaking effectively. As the largest populations live along and south of the MFT, this is one of the most pressing, societally relevant issues for Himalayan earthquakes, but answering it might not be possible except by observation of surface-rupturing events.

Future directions. Future advances in understanding Himalayan tectonics and seismicity will depend on combining existing and rapidly increasing streams of observational data, which should be supported by numerical modelling and laboratory experiments (FIG. 7). Understanding the relevant physics at each of the characteristic scales is crucial, as it motivates new observational techniques and allows the development of advanced physics-based numerical simulations. With increasing satellite observations, geophysical imaging and artificial intelligence techniques, we might be able to identify patterns that are difficult or impossible for humans to detect through traditional methods[198].

The coming decade will see improvements in our ability to observe time-dependent phenomena, such as earthquakes and long-term, non-linear transients (such as slow slip events). Geodetic observations (mainly continuous GPS (cGPS) and InSAR) of ground surface deformation and other remote sensing techniques are becoming increasingly more accurate[199] (FIG. 7). However, their capacity to resolve low, heterogeneous interseismic strain is fundamentally limited by the density of observations (cGPS) and the coherence loss over time owing to vegetation and erosion (InSAR). Furthermore, atmospheric noise (for satellite observations), restricted access to data (for some geophysical networks) and the vast spatial extent of the Himalaya could make advancements challenging.

As there are inherent limitations in seismic cycle observations, future observations, techniques and community initiatives should target the issue of how shortening is partitioned along-strike. At shorter timescales, future efforts should focus on estimating and interpreting the degree to which the interseismic deformation that we observe at the surface reflects the accumulation of elastic and inelastic strain on faults. Another target includes mapping along-strike variations of the down-dip end of the MHT, which will give insight into where and why elastic strain accumulates and how this affects topography.

Such integrated efforts should improve our ability to understand deformation and earthquake potential in one of the most densely populated seismic regions of the world. We hope that integrated earthquake science will eventually provide actionable assessments of spatially variable hazard[200,201] to guide infrastructure development and enable the construction of earthquake early warning systems on large scales[202–204]. The societal impact of this effort would be multiplied by combining it with more science education initiatives to increase earthquake awareness in the local population[205,206]. Earthquake risk mitigation initiatives must be data-driven, incorporating transdisciplinary work by social scientists, engineers and authorities at all levels.

Published online 2 March 2021

1. Bilham, R. Himalayan earthquakes: a review of historical seismicity and early 21st century slip potential. *Geol. Soc. Spec. Publ.* **483**, 423–482 (2019).
2. Wesnousky, S. G. Great pending Himalaya earthquakes. *Seismol. Res. Lett.* **91**, 3334–3342 (2020).
3. Turcotte, D. & Schubert, G. *Geodynamics* (Cambridge Univ. Press, 2002).
4. Scholz, C. H. *The Mechanics of Earthquakes and Faulting* (Cambridge Univ. Press, 2019).
5. Dal Zilio, L., van Dinther, Y., Gerya, T. V. & Pranger, C. C. Seismic behaviour of mountain belts controlled by plate convergence rate. *Earth Planet. Sci. Lett.* **482**, 81–92 (2018).
6. Molnar, P. & England, P. Late Cenozoic uplift of mountain ranges and global climate change: chicken or egg? *Nature* **346**, 29–34 (1990).
7. Willett, S. D. Orogeny and orography: the effects of erosion on the structure of mountain belts. *J. Geophys. Res. Solid Earth* **104**, 28957–28981 (1999).
8. Burbank, D. et al. Decoupling of erosion and precipitation in the Himalayas. *Nature* **426**, 652–655 (2003).
9. Whipple, K. X. The influence of climate on the tectonic evolution of mountain belts. *Nat. Geosci.* **2**, 97–104 (2009).
10. Whittaker, A. C. How do landscapes record tectonics and climate? *Lithosphere* **4**, 160–164 (2012).
11. Molnar, P., England, P. & Martinod, J. Mantle dynamics, uplift of the Tibetan Plateau, and the Indian Monsoon. *Rev. Geophys.* **31**, 357–396 (1993).
12. Zhisheng, A., Kutzbach, J. E., Prell, W. L. & Porter, S. C. Evolution of Asian monsoons and phased uplift of the Himalaya–Tibetan plateau since Late Miocene times. *Nature* **411**, 62–66 (2001).
13. Powell, C. M. A. & Conaghan, P. Plate tectonics and the Himalayas. *Earth Planet. Sci. Lett.* **20**, 1–12 (1973).
14. Molnar, P. & Tapponnier, P. Cenozoic tectonics of Asia: effects of a continental collision. *Science* **189**, 419–426 (1975).

15. Tapponnier, P., Peltzer, G., Le Dain, A., Armijo, R. & Cobbold, P. Propagating extrusion tectonics in Asia: New insights from simple experiments with plasticine. *Geology* **10**, 611–616 (1982).
16. Yin, A. & Harrison, T. M. Geologic evolution of the Himalayan-Tibetan orogen. *Annu. Rev. Earth Planet. Sci.* **28**, 211–280 (2000).
17. Avouac, J.-P. Mountain building: from earthquakes to geologic deformation. *Treatise Geophys.* **6**, 381–432 (2015).
18. Avouac, J.-P. & Tapponnier, P. Kinematic model of active deformation in central Asia. *Geophys. Res. Lett.* **20**, 895–898 (1993).
19. Copley, A., Avouac, J.-P. & Royer, J.-Y. India-Asia collision and the Cenozoic slowdown of the Indian plate: Implications for the forces driving plate motions. *J. Geophys. Res. Solid Earth* **115**, B03410 (2010).
20. Cande, S. C. & Stegman, D. R. Indian and African plate motions driven by the push force of the Réunion plume head. *Nature* **475**, 47–52 (2011).
21. de Sigoyer, J. et al. Dating the Indian continental subduction and collisional thickening in the northwest Himalaya: Multichronology of the Tso Morari eclogites. *Geology* **28**, 487–490 (2000).
22. Ding, L., Kapp, P. & Wan, X. Paleocene−Eocene record of ophiolite obduction and initial India-Asia collision, south central Tibet. *Tectonics* **24**, TC3001 (2005).
23. Patriat, P. & Achache, J. India−Eurasia collision chronology has implications for crustal shortening and driving mechanism of plates. *Nature* **311**, 615–621 (1984).
24. Pusok, A. E. & Stegman, D. R. The convergence history of India-Eurasia records multiple subduction dynamics processes. *Sci. Adv.* **6**, eaaz8681 (2020).
25. DeMets, C., Merkouriev, S. & Jade, S. High-resolution reconstructions and GPS estimates of India−Eurasia and India−Somalia plate motions: 20 Ma to the present. *Geophys. J. Int.* **220**, 1149–1171 (2020).
26. Molnar, P. & Stock, J. M. Slowing of India's convergence with Eurasia since 20 Ma and its

implications for Tibetan mantle dynamics. *Tectonics* **28**, TC3001 (2009).
27. Capitanio, F., Morra, G., Goes, S., Weinberg, R. & Moresi, L. India–Asia convergence driven by the subduction of the Greater Indian continent. *Nat. Geosci.* **3**, 136–139 (2010).
28. Burg, J. & Chen, G. Tectonics and structural zonation of southern Tibet, China. *Nature* **311**, 219–223 (1984).
29. Burchfiel, B. C. et al. *The South Tibetan Detachment System, Himalayan Orogen: Extension Contemporaneous With and Parallel to Shortening in a Collisional Mountain Belt* Vol. 269 (Geological Society of America, 1992).
30. Jixiang, Y., Juntao, X., Chengjie, L. & Huan, L. The Tibetan plateau: regional stratigraphic context and previous work. *Philos. Trans. R. Soc. Lond. A Math. Phys. Sci.* **327**, 5–52 (1988).
31. Brookfield, M. The Himalayan passive margin from Precambrian to Cretaceous times. *Sediment. Geol.* **84**, 1–35 (1993).
32. Gansser, A. *Geology of the Himalayas* (Interscience, 1964).
33. Schelling, D. & Arita, K. Thrust tectonics, crustal shortening, and the structure of the far-eastern Nepal Himalaya. *Tectonics* **10**, 851–862 (1991).
34. Mugnier, J. L. et al. The Siwaliks of western Nepal: I. Geometry and kinematics. *J. Asian Earth Sci.* **17**, 629–642 (1999).
35. DeCelles, P. G. et al. Stratigraphy, structure, and tectonic evolution of the Himalayan fold-thrust belt in western Nepal. *Tectonics* **20**, 487–509 (2001).
36. Meigs, A. J., Burbank, D. W. & Beck, R. A. Middle-late Miocene (>10 Ma) formation of the Main Boundary thrust in the western Himalaya. *Geology* **23**, 423–426 (1995).
37. Ghoshal, S. et al. Constraining central Himalayan (Nepal) fault geometry through integrated thermochronology and thermokinematic modeling. *Tectonics* **39**, e2020TC006399 (2020).

38. Gansser, A. The geodynamic history of the Himalaya. *Zagros Hindu Kush Himalaya Geodyn. Evol.* **3**, 111–121 (1981).

39. Catlos, E. J. et al. Geochronologic and thermobarometric constraints on the evolution of the Main Central Thrust, central Nepal Himalaya. *J. Geophys. Res. Solid Earth* **106**, 16177–16204 (2001).

40. Robinson, D. et al. Kinematic model for the Main Central thrust in Nepal. *Geology* **31**, 359–362 (2003).

41. Davies, G. F. & Brune, J. N. Regional and global fault slip rates from seismicity. *Nat. Phys. Sci.* **229**, 101–107 (1971).

42. Audet, P., Bostock, M. G., Christensen, N. I. & Peacock, S. M. Seismic evidence for overpressured subducted oceanic crust and megathrust fault sealing. *Nature* **457**, 76–78 (2009).

43. Bollinger, L. et al. Thermal structure and exhumation history of the Lesser Himalaya in central Nepal. *Tectonics* **23**, TC5015 (2004).

44. Robinson, D. M., DeCelles, P. G., Patchett, P. J. & Garzione, C. N. The kinematic evolution of the Nepalese Himalaya interpreted from Nd isotopes. *Earth Planet. Sci. Lett.* **192**, 507–521 (2001).

45. Brown, L. et al. Bright spots, structure, and magmatism in southern Tibet from INDEPTH seismic reflection profiling. *Science* **274**, 1688–1690 (1996).

46. Hauck, M., Nelson, K., Brown, L., Zhao, W. & Ross, A. Crustal structure of the Himalayan orogen at ~90° east longitude from Project INDEPTH deep reflection profiles. *Tectonics* **17**, 481–500 (1998).

47. Boullier, A.-M., France-Lanord, C., Dubessy, J., Adamy, J. & Champenois, M. Linked fluid and tectonic evolution in the High Himalaya mountains (Nepal). *Contrib. Mineral. Petrol.* **107**, 358–372 (1991).

48. Lemonnier, C. et al. Electrical structure of the Himalaya of central Nepal: High conductivity around the mid-crustal ramp along the MHT. *Geophys. Res. Lett.* **26**, 3261–3264 (1999).

49. Hetényi, G. *Evolution of deformation of the Himalayan prism: From imaging to modelling*. PhD thesis, École Normale Supérieure–Université Paris-Sud XI (2007).

50. Nábělek, J. et al. Underplating in the Himalaya-Tibet collision zone revealed by the Hi-CLIMB experiment. *Science* **325**, 1371–1374 (2009).

51. Acton, C., Priestley, K., Mitra, S. & Gaur, V. Crustal structure of the Darjeeling—Sikkim Himalaya and southern Tibet. *Geophys. J. Int.* **184**, 829–852 (2011).

52. Subedi, S. et al. Imaging the Moho and the Main Himalayan Thrust in Western Nepal with receiver functions. *Geophys. Res. Lett.* **45**, 13–222 (2018).

53. Singer, J., Kissling, E., Diehl, T. & Hetényi, G. The underthrusting Indian crust and its role in collision dynamics of the Eastern Himalaya in Bhutan: Insights from receiver function imaging. *J. Geophys. Res. Solid Earth* **122**, 1152–1178 (2017).

54. Duputel, Z. et al. The 2015 Gorkha earthquake: a large event illuminating the Main Himalayan Thrust fault. *Geophys. Res. Lett.* **43**, 2517–2525 (2016).

55. Caldwell, W. B. et al. Characterizing the Main Himalayan Thrust in the Garhwal Himalaya, India with receiver function CCP stacking. *Earth Planet. Sci. Lett.* **367**, 15–27 (2013).

56. Schulte-Pelkum, V. et al. Imaging the Indian subcontinent beneath the Himalaya. *Nature* **435**, 1222–1225 (2005).

57. Cattin, R. & Avouac, J. Modeling mountain building and the seismic cycle in the Himalaya of Nepal. *J. Geophys. Res. Solid Earth* **105**, 13389–13407 (2000).

58. Vergne, J., Cattin, R. & Avouac, J. On the use of dislocations to model interseismic strain and stress build-up at intracontinental thrust faults. *Geophys. J. Int.* **147**, 155–162 (2001).

59. Hoste-Colomer, R., Bollinger, L., Lyon-Caen, H., Burtin, A. & Adhikari, L. Lateral structure variations and transient swarm revealed by seismicity along the Main Himalayan Thrust north of Kathmandu. *Tectonophysics* **714**, 107–116 (2017).

60. Hoste-Colomer, R. et al. Lateral variations of the midcrustal seismicity in western Nepal: Seismotectonic implications. *Earth Planet. Sci. Lett.* **504**, 115–125 (2018).

61. Baillard, C. et al. Automatic analysis of the Gorkha earthquake aftershock sequence: evidences of structurally segmented seismicity. *Geophys. J. Int.* **209**, 1111–1125 (2017).

62. Yamada, M., Kandel, T., Tamaribuchi, K. & Ghosh, A. 3D fault structure inferred from a refined aftershock catalog for the 2015 Gorkha earthquake in Nepal. *Bull. Seismol. Soc. Am.* **110**, 26–37 (2020).

63. Mendoza, M. et al. Duplex in the Main Himalayan Thrust illuminated by aftershocks of the 2015 Mw 7.8 Gorkha earthquake. *Nat. Geosci.* **12**, 1018–1022 (2019).

64. Lavé, J. & Avouac, J.-P. Active folding of fluvial terraces across the Siwaliks Hills, Himalayas of central Nepal. *J. Geophys. Res. Solid Earth* **105**, 5735–5770 (2000).

65. Lavé, J. & Avouac, J. Fluvial incision and tectonic uplift across the Himalayas of central Nepal. *J. Geophys. Res. Solid Earth* **106**, 26561–26591 (2001).

66. Seeber, L. & Gornitz, V. River profiles along the Himalayan arc as indicators of active tectonics. *Tectonophysics* **92**, 335–367 (1983).

67. Malik, J. N. et al. Active fault, fault growth and segment linkage along the Janauri anticline (frontal foreland fold), NW Himalaya, India. *Tectonophysics* **483**, 327–343 (2010).

68. Wesnousky, S. G., Kumar, S., Mohindra, R. & Thakur, V. Uplift and convergence along the Himalayan Frontal Thrust of India. *Tectonics* **18**, 967–976 (1999).

69. Almeida, R. V., Hubbard, J., Liberty, L., Foster, A. & Sapkota, S. N. Seismic imaging of the Main Frontal Thrust in Nepal reveals a shallow décollement and blind thrusting. *Earth Planet. Sci. Lett.* **494**, 216–225 (2018).

70. Bollinger, L. et al. Estimating the return times of great Himalayan earthquakes in eastern Nepal: Evidence from the Patu and Bardibas strands of the Main Frontal Thrust. *J. Geophys. Res. Solid Earth* **119**, 7123–7163 (2014).

71. Ader, T. et al. Convergence rate across the Nepal Himalaya and interseismic coupling on the Main Himalayan Thrust: Implications for seismic hazard. *J. Geophys. Res. Solid Earth* **117**, B04403 (2012).

72. Bettinelli, P. et al. Plate motion of India and interseismic strain in the Nepal Himalaya from GPS and DORIS measurements. *J. Geodesy* **80**, 567–589 (2006).

73. Bilham, R., Larson, K. & Freymueller, J. GPS measurements of present-day convergence across the Nepal Himalaya. *Nature* **386**, 61–64 (1997).

74. Chen, Q. et al. A deforming block model for the present-day tectonics of Tibet. *J. Geophys. Res. Solid Earth* **109**, B01403 (2004).

75. Jouanne, F. et al. Oblique convergence in the Himalayas of western Nepal deduced from preliminary results of GPS measurements. *Geophys. Res. Lett.* **26**, 1933–1936 (1999).

76. Wang, Q. et al. Present-day crustal deformation in China constrained by global positioning system measurements. *Science* **294**, 574–577 (2001).

77. Wang, M. & Shen, Z.-K. Present-day crustal deformation of continental China derived from GPS and its tectonic implications. *J. Geophys. Res. Solid Earth* **125**, e2019JB018774 (2020).

78. Stevens, V. & Avouac, J. Interseismic coupling on the main Himalayan thrust. *Geophys. Res. Lett.* **42**, 5828–5837 (2015).

79. Li, S. et al. Geodetic imaging mega-thrust coupling beneath the Himalaya. *Tectonophysics* **747**, 225–238 (2018).

80. Wang, K., Hu, Y. & He, J. Deformation cycles of subduction earthquakes in a viscoelastic Earth. *Nature* **484**, 327–332 (2012).

81. Avouac, J.-P. From geodetic imaging of seismic and aseismic fault slip to dynamic modeling of the seismic cycle. *Annu. Rev. Earth Planet. Sci.* **43**, 233–271 (2015).

82. Stevens, V. & Avouac, J.-P. Millenary M_w > 9.0 earthquakes required by geodetic strain in the Himalaya. *Geophys. Res. Lett.* **43**, 1118–1123 (2016).

83. Almeida, R. et al. Can the updip limit of frictional locking on megathrusts be detected geodetically? Quantifying the effect of stress shadows on near-trench coupling. *Geophys. Res. Lett.* **45**, 4754–4763 (2018).

84. Dal Zilio, L., Jolivet, R. & van Dinther, Y. Segmentation of the Main Himalayan Thrust illuminated by Bayesian inference of interseismic coupling. *Geophys. Res. Lett.* **47**, e2019GL086424 (2020).

85. Yadav, R. K. et al. Strong seismic coupling underneath Garhwal–Kumaun region, NW Himalaya, India. *Earth Planet. Sci. Lett.* **506**, 8–14 (2019).

86. Sreejith, K. et al. Audit of stored strain energy and extent of future earthquake rupture in central Himalaya. *Sci. Rep.* **8**, 16697 (2018).

87. Ponraj, M. et al. Estimation of strain distribution using GPS measurements in the Kumaun region of Lesser Himalaya. *J. Asian Earth Sci.* **39**, 658–667 (2010).

88. Marechal, A. et al. Evidence of interseismic coupling variations along the Bhutan Himalayan arc from new GPS data. *Geophys. Res. Lett.* **43**, 12,399–12,406 (2016).

89. Bilham, R., Mencin, D., Bendick, R. & Bürgmann, R. Implications for elastic energy storage in the Himalaya from the Gorkha 2015 earthquake and other incomplete ruptures of the Main Himalayan Thrust. *Quat. Int.* **462**, 3–21 (2017).

90. Bollinger, L., Avouac, J., Cattin, R. & Pandey, M. Stress buildup in the Himalaya. *J. Geophys. Res. Solid Earth* **109**, B11405 (2004).

91. Bilham, R. Slow tilt reversal of the Lesser Himalaya between 1862 and 1992 at 78°E, and bounds to the southeast rupture of the 1905 Kangra earthquake. *Geophys. J. Int.* **144**, 713–728 (2001).

92. Seeber, L. & Armbruster, J. G. Great detachment earthquakes along the Himalayan arc and long-term forecasting. *Earthq. Pred. Int. Rev.* **4**, 259–277 (1981).

93. Avouac, J.-P., Ayoub, F., Leprince, S., Konca, O. & Helmberger, D. V. The 2005, M_w 7.6 Kashmir earthquake: Sub-pixel correlation of ASTER images and seismic waveforms analysis. *Earth Planet. Sci. Lett.* **249**, 514–528 (2006).

94. Nakata, T., Kumura, K. & Rockwell, T. First successful paleoseismic trench study on active faults in the Himalaya. *Eos Trans. AGU* **79**, 459–486 (1998).

95. Arora, S. & Malik, J. N. Overestimation of the earthquake hazard along the Himalaya: constraints in bracketing of medieval earthquakes from paleoseismic studies. *Geosci. Lett.* **4**, 19 (2017).

96. Lavé, J. et al. Evidence for a great medieval earthquake (~1100 A.D.) in the central Himalayas, Nepal. *Science* **307**, 1302–1305 (2005).

97. Wesnousky, S. G. et al. Geological observations on large earthquakes along the Himalayan frontal fault near Kathmandu, Nepal. *Earth Planet. Sci. Lett.* **457**, 366–375 (2017).

98. Wesnousky, S. G., Kumahara, Y., Chamlagain, D. & Neupane, P. C. Large Himalayan Frontal Thrust paleoearthquake at Khayarmara in eastern Nepal. *J. Asian Earth Sci.* **174**, 346–351 (2019).

99. Pant, M. R. A step toward a historical seismicity of Nepal. *Adarsa* **2**, 29–60 (2002).

100. Sapkota, S. et al. Primary surface ruptures of the great Himalayan earthquakes in 1934 and 1255. *Nat. Geosci.* **6**, 71–76 (2013).

101. Bollinger, L., Tapponnier, P., Sapkota, S. & Klinger, Y. Slip deficit in central Nepal: Omen for a repeat of the 1344 AD earthquake? *Earth Planets Space* **68**, 12 (2016).

102. Yule, D., Dawson, S., Lave, J., Sapkota, S. & Tiwari, D. Possible evidence for surface rupture of the Main Frontal Thrust during the great 1505 Himalayan earthquake, far-western Nepal. In *AGU Fall Meeting* abstract S33C-05 (2006).

103. Bilham, R., Gaur, V. K. & Molnar, P. Himalayan seismic hazard. *Science* **293**, 1442–1444 (2001).

104. Ghazoui, Z. et al. Potentially large post-1505 AD earthquakes in western Nepal revealed by a lake sediment record. *Nat. Commun.* **10**, 2258 (2019).

105. Bilham, R. & England, P. Plateau 'pop-up' in the great 1897 Assam earthquake. *Nature* **410**, 806–809 (2001).

106. England, P. & Bilham, R. The Shillong Plateau and the great 1897 Assam earthquake. *Tectonics* **34**, 1792–1812 (2015).

107. Coudurier-Curveur, A. et al. A composite rupture model for the great 1950 Assam earthquake across the cusp of the East Himalayan Syntaxis. *Earth Planet. Sci. Lett.* **531**, 115928 (2020).

108. Wallace, K., Bilham, R., Blume, F., Gaur, V. & Gahalaut, V. Surface deformation in the region of the 1905 Kangra Mw = 7.8 earthquake in the period 1846–2001. *Geophys. Res. Lett.* **32**, L15307 (2005).

109. Avouac, J.-P., Meng, L., Wei, S., Wang, T. & Ampuero, J.-P. Lower edge of locked Main Himalayan Thrust unzipped by the 2015 Gorkha earthquake. *Nat. Geosci.* **8**, 708–711 (2015).

110. Galetzka, J. et al. Slip pulse and resonance of the Kathmandu basin during the 2015 Gorkha earthquake, Nepal. *Science* **349**, 1091–1095 (2015).

111. Adhikari, L. et al. The aftershock sequence of the 2015 April 25 Gorkha–Nepal earthquake. *Geophys. Suppl. Mon. Not. R. Astron. Soc.* **203**, 2119–2124 (2015).

112. Bai, L. et al. Lateral variation of the Main Himalayan Thrust controls the rupture length of the 2015 Gorkha earthquake in Nepal. *Sci. Adv.* **5**, eaav0723 (2019).

113. Lindsey, E. O. et al. Line-of-sight displacement from ALOS-2 interferometry: M_w 7.8 Gorkha Earthquake and M_w 7.3 aftershock. *Geophys. Res. Lett.* **42**, 6655–6661 (2015).

114. Zuo, R., Qu, C., Shan, X., Zhang, G. & Song, X. Coseismic deformation fields and a fault slip model for the Mw7.8 mainshock and Mw7.3 aftershock of the Gorkha-Nepal 2015 earthquake derived from Sentinel-1A SAR interferometry. *Tectonophysics* **686**, 158–169 (2016).

115. Wang, K. & Fialko, Y. Slip model of the 2015 M_w 7.8 Gorkha (Nepal) earthquake from inversions of ALOS-2 and GPS data. *Geophys. Res. Lett.* **42**, 7452–7458 (2015).

116. Grandin, R. et al. Rupture process of the M_w = 7.9 2015 Gorkha earthquake (Nepal): insights into Himalayan megathrust segmentation. *Geophys. Res. Lett.* **42**, 8373–8382 (2015).

117. Elliott, J. et al. Himalayan megathrust geometry and relation to topography revealed by the Gorkha earthquake. *Nat. Geosci.* **9**, 174–180 (2016).

118. Hubbard, J. et al. Structural segmentation controlled the 2015 M_w 7.8 Gorkha earthquake rupture in Nepal. *Geology* **44**, 639–642 (2016).

119. Whipple, K. X., Shirzaei, M., Hodges, K. V. & Arrowsmith, J. R. Active shortening within the Himalayan orogenic wedge implied by the 2015 Gorkha earthquake. *Nat. Geosci.* **9**, 711–716 (2016).

120. Karplus, M. S. et al. A rapid response network to record aftershocks of the 2015 M 7.8 Gorkha earthquake in Nepal. *Seismol. Res. Lett.* **91**, 2399–2408 (2020).

121. Dal Zilio, L., van Dinther, Y., Gerya, T. & Avouac, J.-P. Bimodal seismicity in the Himalaya controlled by fault friction and geometry. *Nat. Commun.* **10**, 48 (2019).

122. Grandin, R. et al. Long-term growth of the Himalaya inferred from interseismic InSAR measurement. *Geology* **40**, 1059–1062 (2012).

123. Mencin, D. et al. Himalayan strain reservoir inferred from limited afterslip following the Gorkha earthquake. *Nat. Geosci.* **9**, 533–537 (2016).

124. Gualandi, A. et al. Pre- and post-seismic deformation related to the 2015, M_w 7.8 Gorkha earthquake, Nepal. *Tectonophysics* **714–715**, 90–106 (2017).

125. Qiu, Q. et al. The mechanism of partial rupture of a locked megathrust: the role of fault morphology. *Geology* **44**, 875–878 (2016).

126. Pandey, M., Tandukar, R., Avouac, J., Lave, J. & Massot, J. Interseismic strain accumulation on the Himalayan crustal ramp (Nepal). *Geophys. Res. Lett.* **22**, 751–754 (1995).

127. Herman, F. et al. Exhumation, crustal deformation, and thermal structure of the Nepal Himalaya derived from the inversion of thermochronological and thermobarometric data and modeling of the topography. *J. Geophys. Res. Solid Earth* **115**, B06407 (2010).

128. Dal Zilio, L., Ruh, J. & Avouac, J.-P. Structural evolution of orogenic wedges: interplay between erosion and weak décollements. *Tectonics* **39**, e2020TC006210 (2020).

129. Shen, L. et al. Tectonic underplating versus out-of-sequence thrusting beneath the Lesser Himalaya: Insights from the analogue modeling of the Nepal Himalaya fold-and-thrust belt. *J. Asian Earth Sci.* **198**, 104167 (2020).

130. Jackson, M. & Bilham, R. Constraints on Himalayan deformation inferred from vertical velocity fields in Nepal and Tibet. *J. Geophys. Res.* **99**, 13–897 (1994).

131. Alvizuri, C. & Hetényi, G. Source mechanism of a lower crust earthquake beneath the Himalayas and its possible relation to metamorphism. *Tectonophysics* **769**, 128153 (2019).

132. Schulte-Pelkum, V. et al. Mantle earthquakes in the Himalayan collision zone. *Geology* **47**, 815–819 (2019).

133. Bollinger, L. et al. Seasonal modulation of seismicity in the Himalaya of Nepal. *Geophys. Res. Lett.* **34**, L08304 (2007).

134. Lindsey, E. O. et al. Structural control on downdip locking extent of the Himalayan megathrust. *J. Geophys. Res. Solid Earth* **123**, 5265–5278 (2018).

135. Blanpied, M. L., Lockner, D. A. & Byerlee, J. D. Frictional slip of granite at hydrothermal conditions. *J. Geophys. Res. Solid Earth* **100**, 13045–13064 (1995).

136. Marone, C. Laboratory-derived friction laws and their application to seismic faulting. *Annu. Rev. Earth Planet. Sci.* **26**, 643–696 (1998).

137. Fan, W. & Shearer, P. M. Detailed rupture imaging of the 25 April 2015 Nepal earthquake using teleseismic *P* waves. *Geophys. Res. Lett.* **42**, 5744–5752 (2015).

138. Yue, H. et al. Depth varying rupture properties during the 2015 Mw 7.8 Gorkha (Nepal) earthquake. *Tectonophysics* **714**, 44–54 (2017).

139. Michel, S., Avouac, J.-P., Lapusta, N. & Jiang, J. Pulse-like partial ruptures and high-frequency radiation at creeping-locked transition during megathrust earthquakes. *Geophys. Res. Lett.* **44**, 8345–8351 (2017).

140. Wang, X., Wei, S. & Wu, W. Double-ramp on the Main Himalayan Thrust revealed by broadband waveform modeling of the 2015 Gorkha earthquake sequence. *Earth Planet. Sci. Lett.* **473**, 83–93 (2017).

141. Mahadevan, L., Bendick, R. & Liang, H. Why subduction zones are curved. *Tectonics* **29**, TC6002 (2010).

142. Hetényi, G. et al. Segmentation of the Himalayas as revealed by arc-parallel gravity anomalies. *Sci. Rep.* **6**, 33866 (2016).

143. Geological Survey of India, Dasgupta, S., Narula, P., Acharyya, S. K. & Banerjee, J. *Seismotectonic Atlas of India and its Environs* (Geological Survey of India, 2000).

144. Grujic, D. et al. Stress transfer and connectivity between the Bhutan Himalaya and the Shillong Plateau. *Tectonophysics* **744**, 322–332 (2018).

145. Duncan, C., Masek, J. & Fielding, E. How steep are the Himalaya? Characteristics and implications of along-strike topographic variations. *Geology* **31**, 75–78 (2003).

146. Armijo, R., Tapponnier, P., Mercier, J. & Han, T.-L. Quaternary extension in southern Tibet: Field observations and tectonic implications. *J. Geophys. Res. Solid Earth* **91**, 13803–13872 (1986).

147. De, R. & Kayal, J. Seismotectonic model of the Sikkim Himalaya: constraint from microearthquake surveys. *Bull. Seismol. Soc. Am.* **93**, 1395–1400 (2003).

148. Dasgupta, S., Mukhopadhyay, M. & Nandy, D. Active transverse features in the central portion of the Himalaya. *Tectonophysics* **136**, 255–264 (1987).

149. Murphy, M. A. et al. Limit of strain partitioning in the Himalaya marked by large earthquakes in western Nepal. *Nat. Geosci.* **7**, 38–42 (2014).

150. Diehl, T. et al. Seismotectonics of Bhutan: Evidence for segmentation of the Eastern Himalayas and link to foreland deformation. *Earth Planet. Sci. Lett.* **471**, 54–64 (2017).

151. Kumar, A., Mitra, S. & Suresh, G. Seismotectonics of the eastern Himalayan and Indo-Burman plate boundary systems. *Tectonics* **34**, 2279–2295 (2015).

152. Vernant, P. et al. Clockwise rotation of the Brahmaputra Valley relative to India: Tectonic convergence in the eastern Himalaya, Naga Hills, and Shillong Plateau. *J. Geophys. Res. Solid Earth* **119**, 6558–6571 (2014).

153. Barman, P., Ray, J. D., Kumar, A., Chowdhury, J. & Mahanta, K. Estimation of present-day inter-seismic deformation in Kopili fault zone of north-east India using GPS measurements. *Geomatics Nat. Hazards Risk* **7**, 586–599 (2016).

154. Gahalaut, V. & Kundu, B. Possible influence of subducting ridges on the Himalayan arc and on the ruptures of great and major Himalayan earthquakes. *Gondwana Res.* **21**, 1080–1088 (2012).

155. Duvall, M. J., Waldron, J. W., Godin, L. & Najman, Y. Active strike-slip faults and an outer frontal thrust in the Himalayan foreland basin. *Proc. Natl Acad. Sci. USA* **117**, 17615–17621 (2020).

156. Lyon-Caen, H. & Molnar, P. Gravity anomalies, flexure of the Indian plate, and the structure, support and evolution of the Himalaya and Ganga Basin. *Tectonics* **4**, 513–538 (1985).

157. Lyon-Caen, H. & Molnar, P. Constraints on the structure of the Himalaya from an analysis of gravity anomalies and a flexural model of the lithosphere. *J. Geophys. Res. Solid Earth* **88**, 8171–8191 (1983).

158. Cattin, R. et al. Gravity anomalies, crustal structure and thermo-mechanical support of the Himalaya of central Nepal. *Geophys. J. Int.* **147**, 381–392 (2001).

159. Hetényi, G., Cattin, R., Vergne, J. & Nábēˉlek, J. L. The effective elastic thickness of the India Plate from receiver function imaging, gravity anomalies and thermomechanical modelling. *Geophys. J. Int.* **167**, 1106–1118 (2006).

160. Das, D., Mehra, G., Rao, K. G. C., Roy, A. L. & Narayana, M. S. Bouguer, free-air and magnetic anomalies over north-western Himalayas. *Misc. Publ. Geol. Surv. India* **41**, 141–148 (1979).

161. Banerjee, P. Gravity measurements and terrain corrections using a digital terrain model in the NW Himalaya. *Comput. Geosci.* **24**, 1009–1020 (1998).

162. Martelet, G., Sailhac, P., Moreau, F. & Diament, M. Characterization of geological boundaries using 1-D wavelet transform on gravity data: theory and application to the Himalayas. *Geophysics* **66**, 1116–1129 (2001).

163. Tiwari, V., Rao, M. V., Mishra, D. & Singh, B. Crustal structure across Sikkim, NE Himalaya from new gravity and magnetic data. *Earth Planet. Sci. Lett.* **247**, 61–69 (2006).

164. Berthet, T. et al. Lateral uniformity of India Plate strength over central and eastern Nepal. *Geophys. J. Int.* **195**, 1481–1493 (2013).

165. Hammer, P. et al. Flexure of the India plate underneath the Bhutan Himalaya. *Geophys. Res. Lett.* **40**, 4225–4230 (2013).

166. Hubbard, J., Shaw, J. H. & Klinger, Y. Structural setting of the 2008 Mw 7.9 Wenchuan, China, earthquake. *Bull. Seismol. Soc. Am.* **100**, 2713–2735 (2010).

167. Van Hinsbergen, D. J. et al. Restoration of Cenozoic deformation in Asia and the size of Greater India. *Tectonics* **30**, TC5003 (2011).

168. Zuza, A. V., Cheng, X. & Yin, A. Testing models of Tibetan Plateau formation with Cenozoic shortening estimates across the Qilian Shan–Nan Shan thrust belt. *Geosphere* **12**, 501–532 (2016).

169. Meng, J. et al. Reduced convergence within the Tibetan Plateau by 26 Ma? *Geophys. Res. Lett.* **44**, 6624–6632 (2017).

170. DeCelles, P. G., Robinson, D. M. & Zandt, G. Implications of shortening in the Himalayan fold-thrust belt for uplift of the Tibetan Plateau. *Tectonics* **21**, 12-1–12-25 (2002).

171. Robinson, D. M., DeCelles, P. G. & Copeland, P. Tectonic evolution of the Himalayan thrust belt in western Nepal: Implications for channel flow models. *Geol. Soc. Am. Bull.* **118**, 865–885 (2006).

172. McQuarrie, N. et al. Preliminary stratigraphic and structural architecture of Bhutan: implications for the along strike architecture of the Himalayan system. *Earth Planet. Sci. Lett.* **272**, 105–117 (2008).

173. Long, S., McQuarrie, N., Tobgay, T. & Grujic, D. Geometry and crustal shortening of the Himalayan fold-thrust belt, eastern and central Bhutan. *Bulletin* **123**, 1427–1447 (2011).

174. Webb, A. A. G. Preliminary balanced palinspastic reconstruction of Cenozoic deformation across the Himachal Himalaya (northwestern India). *Geosphere* **9**, 572–587 (2013).

175. Ding, L. et al. Quantifying the rise of the Himalaya orogen and implications for the South Asian monsoon. *Geology* **45**, 215–218 (2017).

176. Xu, Q. et al. Stable isotopes reveal southward growth of the Himalayan-Tibetan Plateau since the Paleocene. *Gondwana Res.* **54**, 50–61 (2018).

177. Gébelin, A. et al. The miocene elevation of Mount Everest. *Geology* **41**, 799–802 (2013).

178. Clift, P. D. et al. Correlation of Himalayan exhumation rates and Asian monsoon intensity. *Nat. Geosci.* **1**, 875–880 (2008).

179. Godard, V. et al. Dominance of tectonics over climate in Himalayan denudation. *Geology* **42**, 243–246 (2014).

180. Hodges, K. V., Wobus, C., Ruhl, K., Schildgen, T. & Whipple, K. Quaternary deformation, river steepening, and heavy precipitation at the front of the Higher Himalayan ranges. *Earth Planet. Sci. Lett.* **220**, 379–389 (2004).

181. DeCelles, P. G. et al. Neogene foreland basin deposits, erosional unroofing, and the kinematic history of the Himalayan fold-thrust belt, western Nepal. *Geol. Soc. Am. Bull.* **110**, 2–21 (1998).

182. Bollinger, L., Henry, P. & Avouac, J. Mountain building in the Nepal Himalaya: thermal and kinematic model. *Earth Planet. Sci. Lett.* **244**, 58–71 (2006).

183. Khanal, S. & Robinson, D. M. Upper crustal shortening and forward modeling of the Himalayan thrust belt along the Budhi-Gandaki River, central Nepal. *Int. J. Earth Sci.* **102**, 1871–1891 (2013).

184. Srivastava, P. & Mitra, G. Thrust geometries and deep structure of the outer and lesser Himalaya, Kumaon and Garhwal (India): Implications for evolution of the Himalayan fold-and-thrust belt. *Tectonics* **13**, 89–109 (1994).

185. Fan, S. & Murphy, M. A. Three-dimensional strain accumulation and partitioning in an arcuate orogenic wedge: an example from the Himalaya. *Bulletin* **133**, 3–18 (2021).

186. Shimizu, K., Yagi, Y., Okuwaki, R. & Fukahata, Y. Construction of fault geometry by finite-fault inversion of teleseismic data. *Geophys. J. Int.* **224**, 1003–1014 (2021).

REVIEWS

187. Okada, Y. Internal deformation due to shear and tensile faults in a half-space. *Bull. Seismol. Soc. Am.* **82**, 1018–1040 (1992).

188. Langer, L., Ragon, T., Sladen, A. & Tromp, J. Impact of topography on earthquake static slip estimates. *Tectonophysics* **791**, 228566 (2020).

189. Wang, K. & Fialko, Y. Observations and modeling of coseismic and postseismic deformation due to the 2015 M_w 7.8 Gorkha (Nepal) earthquake. *J. Geophys. Res. Solid Earth* **123**, 761–779 (2018).

190. Ingleby, T., Wright, T., Hooper, A., Craig, T. & Elliott, J. Constraints on the geometry and frictional properties of the Main Himalayan Thrust using coseismic, postseismic, and interseismic deformation in Nepal. *J. Geophys. Res. Solid Earth* **125**, e2019JB019201 (2020).

191. Drukpa, D., Gautier, S., Cattin, R., Namgay, K. & Le Moigne, N. Impact of near-surface fault geometry on secular slip rate assessment derived from uplifted river terraces: implications for convergence accommodation across the frontal thrust in southern Central Bhutan. *Geophys. J. Int.* **212**, 1315–1330 (2018).

192. Meade, B. J. The signature of an unbalanced earthquake cycle in Himalayan topography? *Geology* **38**, 987–990 (2010).

193. Yue, L.-F., Suppe, J. & Hung, J.-H. Structural geology of a classic thrust belt earthquake: the 1999 Chi-Chi earthquake Taiwan (M_w=7.6). *J. Struct. Geol.* **27**, 2058–2083 (2005).

194. Tsukahara, K. & Takada, Y. Aseismic fold growth in southwestern Taiwan detected by InSAR and GNSS. *Earth Planets Space* **70**, 52 (2018).

195. Suppe, J. Geometry and kinematics of fault-bend folding. *Am. J. Sci.* **283**, 684–721 (1983).

196. Rizza, M. et al. Post earthquake aggradation processes to hide surface ruptures in thrust systems: the M8.3, 1934, Bihar-Nepal earthquake ruptures at Charnath Khola (Eastern Nepal). *J. Geophys. Res. Solid Earth* **124**, 9182–9207 (2019).

197. Rajendran, C., John, B., Rajendran, K. & Sanwal, J. Liquefaction record of the great 1934 earthquake predecessors from the north Bihar alluvial plains of India. *J. Seismol.* **20**, 733–745 (2016).

198. Kong, Q. et al. Machine learning in seismology: turning data into insights. *Seismol. Res. Lett.* **90**, 3–14 (2019).

199. Elliott, J. R., Walters, R. J. & Wright, T. J. The role of space-based observation in understanding and responding to active tectonics and earthquakes. *Nat. Commun.* **7**, 13844 (2016).

200. Stevens, V. L., Shrestha, S. N. & Maharjan, D. K. Probabilistic seismic hazard assessment of Nepal. *Bulletin of the Seismological Society of America* **108**, 3488–3510 (2018).

201. Stevens, V. L., De Risi, R., Le Roux-Mallouf, R., Drukpa, D. & Hetényi, G. Seismic hazard and risk in Bhutan. *Natural Hazards* **104**, 2339–2367 (2020).

202. Chamoli, B. P. et al. A prototype earthquake early warning system for northern India. *J. Earthq. Eng.* https://doi.org/10.1080/13632469.2019.1625828 (2019).

203. Mittal, H., Wu, Y.-M., Sharma, M. L., Yang, B. M. & Gupta, S. Testing the performance of earthquake early warning system in northern India. *Acta Geophys.* **67**, 59–75 (2019).

204. Kumar, A. et al. in *15th Symposium on Earthquake Engineering* 231–238 (2014).

205. Subedi, S., Hetényi, G., Denton, P. & Sauron, A. Seismology at school in Nepal: a program for educational and citizen seismology through a low-cost seismic network. *Front. Earth Sci.* **8**, 73 (2020).

206. Subedi, S., Hetényi, G. & Shackleton, R. Impact of an educational program on earthquake awareness and preparedness in Nepal. *Geosci. Commun.* **3**, 279–290 (2020).

207. Webb, A. A. G. et al. The Himalaya in 3D: slab dynamics controlled mountain building and monsoon intensification. *Lithosphere* **9**, 637–651 (2017).

208. Kreemer, C., Blewitt, G. & Klein, E. C. A geodetic plate motion and global strain rate model. *Geochem. Geophys. Geosyst.* **15**, 3849–3889 (2014).

209. Zheng, G. et al. Crustal deformation in the India-Eurasia collision zone from 25 years of GPS measurements. *J. Geophys. Res. Solid Earth* **122**, 9290–9312 (2017).

210. Hetényi, G. et al. Joint approach combining damage and paleoseismology observations constrains the 1714 AD Bhutan earthquake at magnitude 8±0.5. *Geophys. Res. Lett.* **43**, 10,695–10,702 (2016).

211. Ekström, G., Nettles, M. & Dziewoński, A. The global CMT project 2004–2010: Centroid-moment tensors for 13,017 earthquakes. *Phys. Earth Planet. Inter.* **200–201**, 1–9 (2012).

212. Monsalve, G. et al. Seismicity and one-dimensional velocity structure of the Himalayan collision zone: Earthquakes in the crust and upper mantle. *J. Geophys. Res. Solid Earth* **111**, B10301 (2006).

213. Sreejith, K. M. et al. Coseismic and early postseismic deformation due to the 25 April 2015, Mw 7.8 Gorkha, Nepal, earthquake from InSAR and GPS measurements. *Geophysical Research Letters*, **43**, 3160–3168 (2016).

Author contributions

All authors contributed to the research, writing, figure preparation and editing of this Review.

Competing interests

The authors declare no competing interests.

Peer review information

Nature Reviews Earth & Environment thanks the anonymous reviewers for their contribution to the peer review of this work.

Publisher's note

Springer Nature remains neutral with regard to jurisdictional claims in published maps and institutional affiliations.